Chapter 1

Ultrastrong Light–Matter Coupling in Semiconductors

Nicolas Marquez Peraca[*], Andrey Baydin[†], Weilu Gao[‡], Motoaki Bamba[§,¶], and Junichiro Kono[*,†,‖]

[*]Department of Physics and Astronomy, Rice University, Houston, TX 77005, USA, [†]Department of Electrical and Computer Engineering, Rice University, Houston, TX 77005, USA, [‡]Department of Electrical and Computer Engineering, University of Utah, Salt Lake City, UT 84112, [§]Department of Physics, Kyoto University, Kyoto 606-8502, Japan, [¶]PRESTO, Japan Science and Technology Agency, Saitama 332-0012, Japan, [‖]Department of Materials Science and NanoEngineering, Rice University, Houston, TX 77005, USA

ABSTRACT

Light and matter can strongly mix together to form hybrid particles called polaritons. In recent years, polaritons in the so-called ultrastrong coupling (USC) regime have attracted much attention both from fundamental and applied points of view. A variety of nonintuitive phenomena and novel ground states with exotic properties have been predicted for systems in the USC regime, some of which have been experimentally realized. In this chapter, we review the current state of this exciting, rapidly developing field, focusing on USC phenomena in engineered semiconductor systems. We start by giving a brief historical survey of the field and describe the motivations to pursue USC studies. We then provide a detailed mathematical description of the existing theoretical models for USC physics, mentioning some of the controversies related to the approximations and assumptions that break down in the USC regime. Furthermore, we describe some of the groundbreaking experiments that have been conducted recently in diverse semiconductor-based platforms such as intraband transitions, plasmon-phonon polaritons, exciton polaritons, magnon polaritons, and magnon-magnon coupled systems, highlighting the new physics revealed. Finally, we end the chapter by mentioning some of the technological applications that are expected to be enabled by USC, especially in connection with modern information technologies such as quantum computing and quantum information processing.

KEYWORDS

ultrastrong coupling, semiconductors, polaritons, magnons, cavity QED, condensed matter physics, quantum computing, quantum technology

1.1 INTRODUCTION

The main scientific question this chapter deals with is: ***What is the nature of the ground state of a condensed matter system that is ultrastrongly coupled with vacuum electromagnetic fields inside a cavity?*** There are a variety of theoretically predicted many-body cavity quantum electrodynamics (QED) effects, states, and phases in *the ultrastrong coupling (USC) regime* [Forn-Díaz et al. (2019), Kockum et al. (2019)], and it is our goal to review these hitherto-unobserved phenomena. Such phenomena can also be utilized for constructing unique protocols for ultrafast gates and ultrasecure state preparation for quantum information processing. Specifically, we provide an overview of the current state of theoretical and experimental studies of cavity QED systems in the USC regime based on semiconductor quantum wells (QWs), graphene, carbon nanotubes (CNTs), and strongly correlated materials.

1.1.1 What is the ultrastrong coupling regime?

In a cavity embedding matter, there are four quantities that jointly characterize different light-matter coupling regimes: ω_c, g, κ, and γ. Here, ω_c is the cavity mode photon angular frequency, and the parameter g is the coupling strength (or constant or rate). The parameter κ is the photon decay rate of the cavity; $\tau_{cav} = \kappa^{-1}$ is the photon lifetime of the cavity, and the cavity quality factor is defined as $Q = \omega_c \tau_{cav}$. The parameter γ is the nonradiative matter decay rate, which is usually the decoherence rate in the case of solids.

The simplest Hamiltonian one can write down for this system is

$$\mathcal{H} = \hbar\omega_c \hat{a}^\dagger \hat{a} + \hbar\omega_a \hat{b}^\dagger \hat{b} + i\hbar g(\hat{a}^\dagger \hat{b} - \hat{b}^\dagger \hat{a}). \tag{1.1}$$

Here, $\hat{a}$ ($\hat{a}^\dagger$) and $\hat{b}$ ($\hat{b}^\dagger$) are the annihilation (creation) operators for cavity photons and matter excitations, respectively. When the matter resonance frequency, ω_a, is equal to the cavity frequency, ω_c, i.e., $\omega_a = \omega_c \equiv \omega_0$, the eigenfrequencies of the coupled system is obtained as $\omega_\pm = \omega_0 \pm g$, corresponding to the lower polariton (LP) and upper polariton (UP). The frequency difference between them, $2g$, is called the vacuum Rabi splitting (VRS).

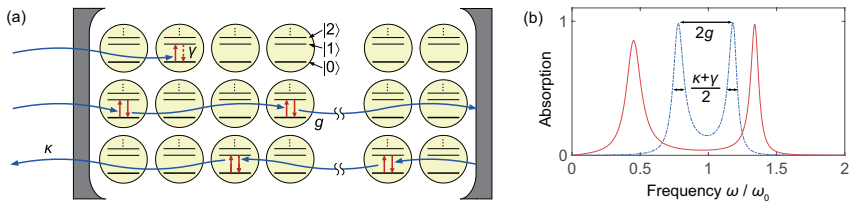

FIGURE 1.1 The parameters that define different light-matter coupling regimes. (a) Sketch of a system consisting of an ensemble of atoms (with multiple levels $|0\rangle$, $|1\rangle$, $|2\rangle$, ...) and a lossy cavity of light. Each atom can be excited by absorbing a photon. A photon is reemitted through relaxation of an atom, while no photon is sometimes emitted by a nonradiative matter decay. g: light-matter coupling rate, γ: matter decay rate, and κ: photon decay rate. (b) Absorption spectra of the cavity system in the SC (blue) and USC (red) regimes in the case of zero detuning $\omega_a = \omega_c = \omega_0$. The SC is defined as $2g > (\gamma + \kappa)/2$, when the VRS is larger than the linewidth. Furthermore, the USC regime arises when g is a significant fraction of the resonance frequency, ω_0.

Strong coupling (**SC**) is achieved when the VRS, $2g$, is larger than the linewidth, $(\kappa + \gamma)/2$; see Fig. 1.1. **USC** is achieved when g becomes a considerable fraction (say, 10%) of ω_0, and some authors define the deep strong coupling (**DSC**) regime as $g/\omega_0 > 1$ [Casanova et al. (2010)]. The two standard figures of merit to measure the coupling strength are

$$C \equiv 4g^2/(\kappa\gamma), \tag{1.2}$$

$$\eta \equiv g/\omega_0. \tag{1.3}$$

Here, C is referred to as the *cooperativity* parameter, which is also the determining factor for the onset of optical bistability through resonant absorption saturation [Bonifacio & Lugiato (1982)], and η is the normalized coupling strength. Using these parameters, the three regimes of light-matter coupling are defined as follows [Forn-Díaz et al. (2019), Kockum et al. (2019)]:

$$\boxed{\textbf{SC} : 2g > (\kappa + \gamma)/2 \text{ (or } C > 1), \textbf{USC} : \eta > 0.1, \text{and } \textbf{DSC} : \eta > 1}$$

Note that the above Hamiltonian, Eq. (1.1), includes only the so-called co-rotating coupling terms, for which the total number of photons and matter excitations is conserved. As is discussed in more detail in Sect. 1.2, this Hamiltonian

is derived under the rotating-wave approximation (RWA). In general, counter-rotating terms (CRTs), $i\hbar g(\hat{a}^\dagger \hat{b}^\dagger - \hat{a}\hat{b})$, also appear in the Hamiltonian and become non-negligible in the USC and DSC regimes, where they play essential roles in inducing non-intuitive physical phenomena.

In Table 1.1, we summarize the commonly used light–matter coupling models (or Hamiltonians). In the Jaynes–Cummings model and the quantum Rabi model, matter, approximated as a single two-level atom (or a two-level quantum dot), couples with a single photonic mode. The difference between the two models is that the former adopts the RWA, i.e., neglects the CRTs, while the latter retains the CRTs. When the matter is instead approximated as multiple two-level atoms, these models are called the Tavis–Cummings model and the Dicke model, respectively. On the other hand, when the matter is approximated as a single bosonic excitation as in Eq. (1.1), the model becomes the Hopfield model, irrespective of whether the RWA is used.

	1 two-level atom	N two-level atoms	Bosonic excitations
Within RWA	Jaynes–Cummings model	Tavis–Cummings model	Hopfield model
Beyond RWA	Quantum Rabi model	Dicke model	Hopfield model

TABLE 1.1 Light-matter coupling Hamiltonians. Under the RWA, the CRTs are neglected in the Hamiltonian.

1.1.2 Why ultrastrong light–matter coupling?

It is important to note that in cavity QED systems in the USC regime the "light field" that the matter strongly couples with is not an external laser field but the vacuum fluctuation field in the cavity. This fact makes USC physics distinctly different from ordinary nonlinear optical phenomena, which require a strong *external* field and thus inevitably involve excited and/or nonequilibrium matter states. In contrast, USC phenomena arise from the properties of the ground state of the matter-vacuum hybrid *in equilibrium*. This new ground state is a matter-vacuum entangled state [Ciuti et al. (2005), Ashhab & Nori (2010), Felicetti et al. (2015)], which has characteristics that neither the original matter ground state nor the usual vacuum possesses.

There is a long history of theoretical studies of USC physics. Early studies focused on the breakdown of the RWA [Bloch & Siegert (1940), Shirley (1965), Cohen-Tannoudji et al. (1973), Allen & Eberly (1975), De Zela et al. (1997)]. After the 1973 discovery of a new type of phase transition, *the superradiant phase transition (SRPT)*, based on the Dicke Hamiltonian [Hepp & Lieb (1973), Wang & Hioe (1973)], attention has been paid to the properties of the ground state and the resultant nonintuitive quantum phenomena: e.g., quantum vacuum radiation [Ciuti et al. (2005), Ciuti & Carusotto (2006), De Liberato et al. (2007), Auer & Burkard (2012), Hagenmüller (2016)] (similar to the Unruh-Hawking radiation from black hole explosions [Unruh (1974), Hawking (1974, 1975), Unruh

(1976), Yablonovitch (1989)]) induced by the dynamic Casimir effect [Moore (1970), Fulling & Davies (1976), Kardar & Golestanian (1999)] or through spontaneous conversion [Stassi et al. (2013)], unusual photon counting statistics [Ridolfo et al. (2012)], the breakdown of the Purcell effect or light-matter "decoupling" [De Liberato (2014), Jaako et al. (2016)], single-photon nonlinear optics [Sanchez-Burillo et al. (2014)], quantum chaos [Emary & Brandes (2003*b*,*a*)], spontaneous parity-symmetry breaking [Bamba et al. (2016)], and ground state electroluminescence [Cirio et al. (2016, 2019)].

For applications, solid-state cavity or circuit QED systems in the USC regime have been recognized to be promising for quantum simulations, simulating, e.g., the quantum Rabi model [Ballester et al. (2012), Mezzacapo et al. (2014), Hwang et al. (2015), Puebla et al. (2017)], Dirac equation physics [Pedernales et al. (2013)], and Dicke physics [Mezzacapo et al. (2014), Lamata (2017)]. Furthermore, the many-body entangled ground states [Ashhab & Nori (2010), Felicetti et al. (2015)] can be used to construct quantum information processing protocols [Wang et al. (2010)] for, e.g., cat-state-based quantum error correction [Ofek et al. (2016)]. Also, ultrafast two-qubit quantum gates have been considered [Romero et al. (2012), Kyaw, Herrera-Martí, Solano, Romero & Kwek (2015), Kyaw, Felicetti, Romero, Solano & Kwek (2015), Wang et al. (2016)]; in particular, Romero et al. (2012) used *ab initio* calculations to demonstrate quantum gates in the USC regime that can be performed at subnanosecond time scales. Finally, Nataf and Ciuti showed that the qubit coherence time and fidelity of a universal set of quantum gates can be dramatically improved in an optimal regime of USC [Nataf & Ciuti (2011)].

Another possible application of USC is the "quantum battery," where quantum coherence or entanglement enhances the stored energy density or the charging power (stored energy over charging time). Ferraro et al. (2018) theoretically suggested that, in the Dicke model, the charging power can be enhanced by factor $\sqrt{N}$ for $N \gg 1$ due to the Dicke cooperativity (inter-atom entanglement mediated by the photonic mode), i.e., the charging time is shortened by $\sqrt{N}$. Further, they also suggested that the stored energy density can be enhanced by rearrangement of charges in the superradiant phase obtained by USC [Ferraro et al. (2019)]. These studies are reviewed by Ferraro et al. (2020).

Finally, it has been proposed that USC may be useful for dark matter detection. An axion haloscope for detecting galactic axions can be improved by the use of magnon–photon USC in a GHz-frequency cavity embedding a yttrium iron garnet (YIG) sphere [Flower, Bourhill, Goryachev & Tobar (2019), Flower, Goryachev, Bourhill & Tobar (2019)]. While many ongoing axion haloscope projects are based on the expected axion–photon interaction, an interaction between axions and electron spins may also exist. Flower, Bourhill, Goryachev & Tobar (2019) reported an experimental setup to detect signals of magnon polaritons excited by axions. The magnon–photon USC enlarges the frequency (energy) range of the haloscope [Flower, Goryachev, Bourhill & Tobar (2019)], which is essential for narrowing the parameter space where axions may exist.

1.1.3 Why solid-state cavity QED systems for USC studies?

In order to maximize C and η, one should construct a cavity QED setup that combines a large dipole moment (i.e., large g), a small decoherence rate (i.e., small γ), a large cavity Q factor (i.e., small κ), and a small resonance frequency ω_0. **Condensed matter (or solid-state) systems have a particular advantage over atomic and molecular systems in achieving large g values.** This is due to the cooperative $\sqrt{N}$-fold enhancement of light-matter coupling, i.e., Dicke cooperativity, expected for an N-body system [Dicke (1954), Kaluzny et al. (1983), Amsüss et al. (2011), Tabuchi et al. (2014), Zhang, Zou, Jiang & Tang (2014)], combined with colossal dipole moments available in solids.

Semiconductor QWs can create clean and tunable solid-state environments with quantum-engineered optical properties. Microcavity exciton polaritons in a QW — a strongly coupled light-condensed-matter system — have exhibited a diverse array of quantum many-body phenomena [Khitrova et al. (1999), Deng et al. (2010), Gibbs et al. (2011)]. However, due to the relatively large values of ω_0, corresponding to the near-infrared and visible ranges, and relatively small dipole moments for interband transitions, it is not practical to achieve large values of $\eta = g/\omega_0$ using QW exciton polaritons.

As detailed in Sect. 1.3.1, *intraband* transitions, including intersubband transitions (ISBTs) [Helm (2000), Paiella (2006)] and cyclotron resonance (CR) [Lax & Mavroides (1960), McCombe & Wagner (1975), Kono (2001), Hilton et al. (2012)], are much better suited for exploring USC phenomena because of their small ω_0, typically in the midinfrared (MIR) and THz range, and large dipole moments. Liu (1997) first proposed and analyzed ISB polaritons theoretically; Ciuti et al. (2005) discussed the nonclassical nature of the ground-state properties of ISB polaritons in the USC regime. The first experimental observation of polariton splitting of ISBTs was reported by Dini et al. (2003), followed by a similar observation by Dupont et al. (2003); these early studies already reported η values >0.01. Progressively higher values of η have since been reported by various experimental groups [Anappara et al. (2005, 2006, 2007), Dupont et al. (2007), Sapienza et al. (2007, 2008), Todorov et al. (2009), Anappara et al. (2009), Günter et al. (2009), Geiser et al. (2010), Todorov, Andrews, Colombelli, De Liberato, Ciuti, Klang, Strasser & Sirtori (2010), Zanotto et al. (2010), Jouy et al. (2011), Geiser et al. (2012), Porer et al. (2012), Zanotto et al. (2012), Delteil et al. (2012), Dietze et al. (2013), Askenazi et al. (2014, 2017), Laurent et al. (2017), Jeannin et al. (2019)].

CR, i.e., inter-Landau-level transitions (ILLTs), has also been used to study strong coupling in two-dimensional electron gases (2DEGs) in semiconductor QWs [Scalari et al. (2012), Muravev et al. (2013), Maissen et al. (2014), Zhang, Lou, Li, Reno, Pan, Watson, Manfra & Kono (2016), Maissen et al. (2017), Bayer et al. (2017)] and on the surface of liquid helium [Abdurakhimov et al. (2016)]. In some of these cases, extremely high values of η (= 0.87 [Maissen et al. (2014)] and = 1.43 [Bayer et al. (2017)]) have been achieved. More recently,

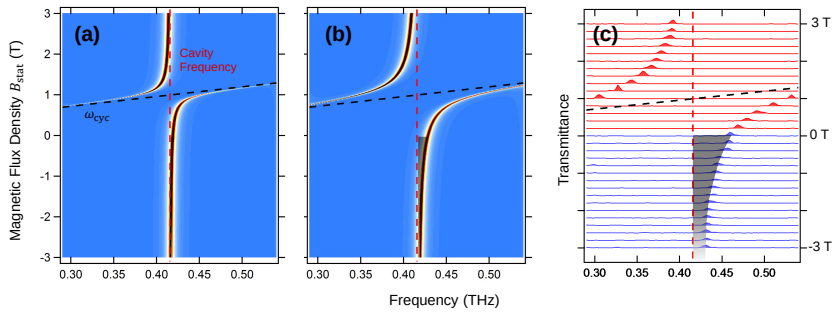

FIGURE 1.2 Vacuum Bloch-Siegert shift of Landau polaritons with ultrahigh cooperativity [Bamba et al. (2019)]. Numerically calculated THz transmission for the CR–cavity system for interaction strength (a) $g/2\pi$ = 37.5 GHz, (b) $g/2\pi$ = 75.0 GHz, and (c) experimental data (interaction strength is estimated as $g/2\pi$ = 150.1 GHz) as a function of frequency $\omega/2\pi$ and external DC magnetic field B_{DC}. Dashed red and black lines show bare cavity and CR frequencies, respectively, without considering their interaction. At $B_{\mathrm{DC}} > 0$, the CR and a circularly polarized probe THz wave are co-rotating and the VRS (anticrossing) is obtained. At $B_{\mathrm{DC}} < 0$, the vacuum BS shift appears due to the counter-rotating coupling between the CR and the circularly polarized cavity field as highlighted by the gray shaded areas.

clear evidence has been obtained for the breakdown of the RWA [Li, Bamba, Zhang, Fallahi, Gardner, Gao, Lou, Yoshioka, Manfra & Kono (2018)], which resulted in a shift in the resonance frequency known as *the Bloch-Siegert (BS) shift* [Bloch & Siegert (1940)]; see Fig. 1.2. The lowest-order term in the BS shift is on the order of g^2/ω_0 [Allen & Eberly (1975)]. Higher-order terms of the BS shift have also been calculated quantum mechanically [Shirley (1965), Cohen-Tannoudji et al. (1973)], which have to be taken into account in order to correctly estimate the magnetic moment values from magnetic resonance experiments [Abragam (1961)]. It should be emphasized that this is a *vacuum* BS shift in a Landau-polariton system, which occurs when the average photon number inside the cavity is much less than one. The shift in this case is caused by **the USC of a Landau-quantized 2DEG with the counter-rotating component of the vacuum fluctuation field inside the cavity**.

1.2 THEORY OF ULTRASTRONG LIGHT–MATTER COUPLING

1.2.1 Hamiltonians and resonance frequencies

When we do not consider the spin degree of freedom, the Hamiltonian describing the electromagnetic fields and charged particles (electrons and ions) is generally expressed by the so-called minimal-coupling Hamiltonian [Cohen-Tannoudji

et al. (1989)]

$$\hat{\mathcal{H}}_v = \int \mathrm{d}\boldsymbol{r} \left[\frac{\varepsilon_0 \hat{\boldsymbol{E}}_\perp(\boldsymbol{r})^2}{2} + \frac{\hat{\boldsymbol{B}}(\boldsymbol{r})^2}{2\mu_0} \right] + \sum_{j=1}^{N} \frac{[\hat{\boldsymbol{p}}_j - e_j \hat{\boldsymbol{A}}(\boldsymbol{r}_j)]^2}{2m_j} + \hat{V}(\{\hat{\boldsymbol{r}}_j\}). \quad (1.4)$$

This is derived in the Coulomb gauge by the Legendre transformation of a Lagrangian describing Maxwell's equations and Newton's equations of motion with the Lorentz force. The first and second terms are the energies of the transverse component of the electric field $\hat{\boldsymbol{E}}_\perp(\boldsymbol{r}) = -\hat{\boldsymbol{\Pi}}(\boldsymbol{r})/\varepsilon_0$ and of the magnetic field $\hat{\boldsymbol{B}}(\boldsymbol{r}) = \boldsymbol{\nabla} \times \hat{\boldsymbol{A}}(\boldsymbol{r})$, respectively. $\hat{\boldsymbol{A}}(\boldsymbol{r})$ is the vector potential, and $\hat{\boldsymbol{\Pi}}(\boldsymbol{r})$ is its conjugate momentum satisfying $[\hat{\boldsymbol{A}}(\boldsymbol{r}), \hat{\boldsymbol{\Pi}}(\boldsymbol{r}')] = \boldsymbol{\delta}_\perp(\boldsymbol{r} - \boldsymbol{r}')$, where $\boldsymbol{\delta}_\perp(\boldsymbol{r}) = \delta(\boldsymbol{r})\mathbf{1} - (2\pi)^{-3} \int \mathrm{d}\boldsymbol{k}\ (\boldsymbol{k}\boldsymbol{k}/k^2)\mathrm{e}^{\mathrm{i}\boldsymbol{k}\cdot\boldsymbol{r}}$ is the dyadic transverse delta function [Cohen-Tannoudji et al. (1989)]. The third term in Eq. (1.4) represents the kinetic energy of the charged particles. $\hat{\boldsymbol{r}}_j$ and $\hat{\boldsymbol{p}}_j$ are, respectively, the position and momentum of the j-th particle with a mass m_j and a charge e_j. They satisfy $[\hat{\boldsymbol{r}}_j, \hat{\boldsymbol{p}}_{j'}] = \mathrm{i}\hbar\delta_{j,j'}\mathbf{1}$. N is the number of the charged particles. The last term in Eq. (1.4) represents the Coulomb interaction. The interaction between the electromagnetic fields and charged particles is obtained by expanding the third term in Eq. (1.4).

We can transform the minimal-coupling Hamiltonian, Eq. (1.4), into different forms. Here, we define the electric polarization as $\hat{\boldsymbol{P}}(\boldsymbol{r}) \equiv \sum_{j=1}^{N} e_j \hat{\boldsymbol{r}}_j \delta(\boldsymbol{r} - \boldsymbol{R}_j)$, where $\boldsymbol{R}_j$ is the position of a lattice site to which the j-th particle belongs. This expression is valid in the long-wavelength approximation, i.e., the distance $|\hat{\boldsymbol{r}}_j - \boldsymbol{R}_j|$ between the particle and the lattice site is much shorter than the wavelength of interest. By using an unitary operator $\hat{U} \equiv \exp[(\mathrm{i}\hbar)^{-1} \int \mathrm{d}\boldsymbol{r}\ \hat{\boldsymbol{A}}(\boldsymbol{r}) \cdot \hat{\boldsymbol{P}}(\boldsymbol{r})]$, we get a different form of Hamiltonian $\hat{\mathcal{H}}_l \equiv \hat{U}\hat{\mathcal{H}}_v\hat{U}^\dagger$ as

$$\hat{\mathcal{H}}_l = \int \mathrm{d}\boldsymbol{r} \left\{ \frac{[\hat{\boldsymbol{D}}(\boldsymbol{r}) - \hat{\boldsymbol{P}}_\perp(\boldsymbol{r})]^2}{2\varepsilon_0} + \frac{\hat{\boldsymbol{B}}(\boldsymbol{r})^2}{2\mu_0} \right\} + \sum_{j=1}^{N} \frac{\hat{\boldsymbol{p}}_j{}^2}{2m_j} + V(\{\hat{\boldsymbol{r}}_j\}), \quad (1.5)$$

where we used the following relations: $\hat{U}\hat{\boldsymbol{\Pi}}(\boldsymbol{r})\hat{U}^\dagger = \hat{\boldsymbol{\Pi}}(\boldsymbol{r}) + \hat{\boldsymbol{P}}_\perp(\boldsymbol{r})$ and $\hat{U}\hat{\boldsymbol{p}}_j\hat{U}^\dagger = \hat{\boldsymbol{p}}_j + e_j\hat{\boldsymbol{A}}(\boldsymbol{R}_j)$ for the transverse component of the electric polarization $\hat{\boldsymbol{P}}_\perp(\boldsymbol{r}) \equiv \int \mathrm{d}\boldsymbol{r}\ \boldsymbol{\delta}_\perp(\boldsymbol{r} - \boldsymbol{r}') \cdot \hat{\boldsymbol{P}}(\boldsymbol{r})$. In this form, the interaction between the electromagnetic fields and charged particles is obtained by expanding the first term in Eq. (1.5), which still represents the energy of the transverse electric field but is described by the electric displacement field $\hat{\boldsymbol{D}}(\boldsymbol{r}) = -\hat{\boldsymbol{\Pi}}(\boldsymbol{r})$ and the trasverse electric polarization $\hat{\boldsymbol{P}}_\perp(\boldsymbol{r})$. The transformation beyond the long-wavelength approximation is known as the Power–Zienau–Woolley transformation [Cohen-Tannoudji et al. (1989)].

Equations (1.4) and (1.5) are said to be in the velocity and length forms, respectively, or sometimes called the Coulomb gauge and the dipole gauge, respectively. These two forms in principle give the same physics in the long-wavelength approximation. However, in calculations of specific systems, we

usually truncate some of the matter levels and electromagnetic modes. For example, as shown in Fig. 1.3, there are in general more than two subbands in the conduction and valence bands and many cavity modes in a Fabry–Pérot (FP) cavity. We usually focus on just two subbands and one cavity mode in a frequency range of interest, and neglect the other levels (subbands) and cavity modes. However, if we perform such truncation, $\mathcal{H}_v$ and $\mathcal{H}_l$ are no longer related to each other through a unitary transform; i.e., they are not equivalent and thus give different dynamics. Such truncation is justified (and thus the two Hamiltonians become approximately equivalent) only when the neglected levels and modes exist far out of the frequency range of interest. However, **in the USC regime, the frequency range of interest becomes extremely large, and the influence of truncation frequently becomes crucial** [Bamba & Ogawa (2016), De Bernardis et al. (2018)].

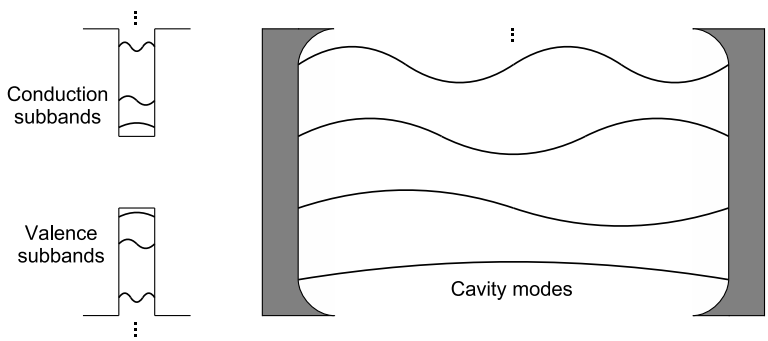

FIGURE 1.3 Sketches of subbands in a semiconductor QW and cavity modes in a FP cavity. In real systems, there can be many subbands in the conduction and valence bands and many cavity modes (as indicated by the three dots in each). However, in theoretical analyses, one usually focuses on only some of the subbands and cavity modes (i.e., truncate the other bands and modes). Such simplification invalidates the unitary transformation between the Hamiltonians in the velocity and length forms.

This truncation issue is related to the so-called *gauge ambiguity* problem, which has attracted much attention in recent years, especially in deriving the Jaynes-Cummings and quantum Rabi models. We can derive these models from both forms of the Hamiltonian by truncation. However, when we compare the eigenfrequencies between the truncated and original Hamiltonians, one form can show better agreement than the other. Then, one faces the question of which form gives a better approximation after truncation is done. As we will see in Sect. 1.2.1.2, the length form usually provides a better approximation in the case of electric dipole transitions. It has recently been pointed out that the velocity form can also give the same level of approximation if we properly transform the Coulomb potential V under truncation [Di Stefano et al. (2019), Garziano et al. (2020)]. On the other hand, it has also been suggested that a much better

approximation can be obtained when one performs truncation in an intermediate form between the velocity and length forms [Stokes & Nazir (2019*a*), Roth et al. (2019)]. The case of time-dependent light–matter interactions has also been discussed [Stokes & Nazir (2019*b*)].

In the following, instead of discussing the ambiguity issues in more detail, we will derive simple Hamiltonians for three cases. In Sect. 1.2.1.1, we provide a general discussion on the quantization of electromagnetic fields. In Sect. 1.2.1.2, ISBTs in semiconductor QWs in the USC regime are theoretically described. In Sect. 1.2.1.3, the physics of optical phonons and excitons in bulk semiconductors in the USC regime is examined. In these two cases, it is known that the length form gives a better convergence than the velocity form for matter-level truncation. In Sect. 1.2.1.4, CR in a 2DEG in a cavity, or Landau polaritons, is described. In this case, the velocity form is suitable for deriving a simple Hamiltonian, and it well explains the experimental results presented in Sect. 1.3 (see also Fig. 1.2).

1.2.1.1 Sum rule and quantization of electromagnetic fields

As a general discussion common to all three cases (ISBTs, phonons/excitons, and CR), let us first define the Hamiltonians of the electromagnetic fields and charged particles, respectively, as

$$\hat{\mathcal{H}}_{\mathrm{em}} = \int \mathrm{d}\boldsymbol{r} \left\{ \frac{\hat{\boldsymbol{\Pi}}(\boldsymbol{r})^2}{2\varepsilon_0\varepsilon_{\mathrm{bg}}} + \frac{[\boldsymbol{\nabla}\times\hat{\boldsymbol{A}}(\boldsymbol{r})]^2}{2\mu_0} \right\}, \tag{1.6a}$$

$$\hat{\mathcal{H}}_{\mathrm{mat}} = \sum_{j=1}^{N} \frac{\hat{\boldsymbol{p}}_j{}^2}{2m_j} + \hat{V}(\{\hat{\boldsymbol{r}}_j\}). \tag{1.6b}$$

Here, we consider a part of the matter as a dielectric medium with a frequency-independent (non-dispersive) relative permittivity $\varepsilon_{\mathrm{bg}}$ and put it into $\hat{\mathcal{H}}_{\mathrm{em}}$. Then, the speed of light in the $\hat{\mathcal{H}}_{\mathrm{em}}$ system is $v \equiv c/\sqrt{\varepsilon_{\mathrm{bg}}}$. The total Hamiltonians in Eqs. (1.4) and (1.5) can then be rewritten as

$$\hat{\mathcal{H}}_v = \hat{\mathcal{H}}_{\mathrm{em}} + \hat{\mathcal{H}}_{\mathrm{mat}} + \sum_{j=1}^{N} \left[-\frac{e_j\hat{\boldsymbol{p}}_j\cdot\hat{\boldsymbol{A}}(\boldsymbol{r}_j)}{m_j} + \frac{e_j{}^2\hat{\boldsymbol{A}}(\boldsymbol{r}_j)^2}{2m_j} \right], \tag{1.7a}$$

$$\hat{\mathcal{H}}_l = \hat{\mathcal{H}}_{\mathrm{em}} + \hat{\mathcal{H}}_{\mathrm{mat}} + \int \mathrm{d}\boldsymbol{r} \left[-\frac{\hat{\boldsymbol{D}}(\boldsymbol{r})\cdot\hat{\boldsymbol{P}}_\perp(\boldsymbol{r})}{\varepsilon_0\varepsilon_{\mathrm{bg}}} + \frac{\hat{\boldsymbol{P}}_\perp(\boldsymbol{r})^2}{2\varepsilon_0\varepsilon_{\mathrm{bg}}} \right]. \tag{1.7b}$$

In each expression, the third term represents the light-matter coupling. The last term in Eq. (1.7a) [Eq. (1.7b)] is called the A^2 [P^2] term or the diamagnetic term.

From the matter Hamiltonian $\hat{\mathcal{H}}_{\mathrm{mat}}$, Eq. (1.6b), together with the relation $(m_j/\hbar^2)[\hat{\boldsymbol{r}}_j, [\hat{\mathcal{H}}_{\mathrm{mat}}, \hat{\boldsymbol{r}}_j]] = \mathbf{1}$, we can derive the following general relation called the Thomas–Reiche–Kuhn (TRK) sum rule [Luttinger & Kohn (1955)]:

$$\sum_n f_{n,i} = 1, \tag{1.8}$$

where $f_{n,i}$ is the oscillator strength for the transition from an initial state (i-th state) to the n-th state and is defined as

$$f_{n,i} \equiv \frac{2m_j\omega_{n,i}}{e_j{}^2\hbar}|\boldsymbol{d}_{n,i}|^2. \tag{1.9}$$

Here, $\omega_{n,i}$ is the frequency difference between the two states, and $\boldsymbol{d}_{n,i} \equiv \langle n|e_j\hat{\boldsymbol{r}}_j|i\rangle$ is the transition dipole moment.

Next, let us rewrite the Hamiltonian $\hat{\mathcal{H}}_{\mathrm{em}}$ of the electromagnetic fields in terms of the annihilation and creation operators of photons. Following the procedure of quantization of the electromagnetic wave in an dielectric medium described by Glauber & Lewenstein (1991), we can write the operators of the vector potential and its conjugate momentum as

$$\hat{\boldsymbol{A}}(\boldsymbol{r}) = \sum_k \sqrt{\frac{\hbar}{2\varepsilon_0\varepsilon_{\mathrm{bg}}\omega_k}}\left[\boldsymbol{\psi}_k^*(\boldsymbol{r})\hat{a}_k^\dagger + \boldsymbol{\psi}_k(\boldsymbol{r})\hat{a}_k\right], \tag{1.10}$$

$$\hat{\boldsymbol{\Pi}}(\boldsymbol{r}) = \sum_k \mathrm{i}\sqrt{\frac{\varepsilon_0\varepsilon_{\mathrm{bg}}\hbar\omega_k}{2}}\left[\boldsymbol{\psi}_k^*(\boldsymbol{r})\hat{a}_k^\dagger - \boldsymbol{\psi}_k(\boldsymbol{r})\hat{a}_k\right]. \tag{1.11}$$

Here, $\hat{a}_k$ is the photon annihilation operator for the k-th mode, satisfying $[\hat{a}_k, \hat{a}_{k'}^\dagger] = \delta_{k,k'}$, ω_k is the eigenfrequency, and $\boldsymbol{\psi}_k(\boldsymbol{r})$ is the wavefunction including the polarization direction. The Hamiltonian of the electromagnetic wave is then rewritten as

$$\hat{\mathcal{H}}_{\mathrm{em}} = \sum_k \hbar\omega_k\left(\hat{a}_k^\dagger\hat{a}_k + \frac{1}{2}\right). \tag{1.12}$$

1.2.1.2 Intersubband transitions

Let us consider an ISBT in a semiconductor QW embedded in a microcavity. From a one-body potential in the QW through the Coulomb interaction $\hat{V}$, subbands for electrons (holes) can be obtained within the conduction (valence) band. We focus on two subbands with a frequency difference of ω_{a} and describe the j-th electron or hole by Pauli operators: $\hat{\sigma}_j^z \equiv |1_j\rangle\langle 1_j| - |0_j\rangle\langle 0_j|$, $\hat{\sigma}_j^+ \equiv |1_j\rangle\langle 0_j|$, $\hat{\sigma}_j^- \equiv |0_j\rangle\langle 1_j|$, $\hat{\sigma}_j^x = \hat{\sigma}_j^+ + \hat{\sigma}_j^-$, and $\hat{\sigma}_j^y = -\mathrm{i}(\hat{\sigma}_j^+ - \hat{\sigma}_j^-)$, where $|0_j\rangle$ and $|1_j\rangle$ represent the lower and upper subband states of the j-th particle, respectively. We assume that the QW is placed in a FP cavity with perfect mirrors, distance L, and area S, for which $\omega_{\mathrm{c}} = v(n\pi/L)$ and $\boldsymbol{\psi} = \boldsymbol{e}_\xi(2/SL)^{1/2}\sin[(n\pi/L)z]\mathrm{e}^{\mathrm{i}\boldsymbol{k}_\parallel\cdot\boldsymbol{r}_\parallel}$ for the n-th cavity mode with in-plane wavevector $\boldsymbol{k}_\parallel$ polarized in the ξ direction.

By neglecting many-body Coulomb interactions (nonlinear responses) in $\hat{V}$ as well as in-plane energy dispersions, we can write the matter Hamiltonian, Eq. (1.6b), as

$$\hat{\mathcal{H}}_{\mathrm{mat}} = \sum_{j=1}^{N}\frac{\hbar\omega_{\mathrm{a}}}{2}\left(\hat{\sigma}_j^z + \frac{1}{2}\right) = \hbar\omega_{\mathrm{a}}\left(\hat{S}_z + \frac{N}{2}\right), \tag{1.13}$$

where $\hat{S}_\xi \equiv \sum_{j=1}^{N} \hat{\sigma}_j^\xi/2$ is a $\frac{N}{2}$-spin operator representing the ensemble of particles. When we focus on just one cavity mode, the Hamiltonians in the two forms, Eqs. (1.7), are rewritten as

$$\hat{\mathcal{H}}_v/\hbar \approx \omega_c \hat{a}^\dagger \hat{a} + \omega_a \left(\hat{S}_z + \frac{N}{2}\right) + \frac{2\bar{g}}{\sqrt{N}} \hat{S}_y (\hat{a}^\dagger + \hat{a}) + D(\hat{a}^\dagger + \hat{a})^2, \tag{1.14a}$$

$$\hat{\mathcal{H}}_l/\hbar \approx \omega_c \hat{a}^\dagger \hat{a} + \omega_a \left(\hat{S}_z + \frac{N}{2}\right) + \frac{\mathrm{i}2\tilde{g}}{\sqrt{N}} \hat{S}_x (\hat{a}^\dagger - \hat{a}) + \frac{4\tilde{g}^2}{N\omega_c} \hat{S}_x{}^2. \tag{1.14b}$$

The coupling strengths appearing in these equations are defined as $\bar{g} \equiv (\omega_a/\omega_c)^{1/2} g$ and $\tilde{g} \equiv (\omega_c/\omega_a)^{1/2} g$, where

$$g \equiv \sqrt{\frac{\omega_a N}{2\hbar \varepsilon_0 \varepsilon_{bg}}}\, |\boldsymbol{d}_{1,0} \cdot \boldsymbol{\psi}(z_{QW})|. \tag{1.15}$$

Here z_{QW} is the z position of the QW. We find that in the velocity form, since $\bar{g} \propto \omega_a$, the coupling strength is larger for a higher subband, which is usually neglected due to truncation in simple analyses. Then, the matter-level truncation is crucial in the velocity form, and the length form, where $\tilde{g}$ is independent of ω_a, usually shows better convergence.

Using the sum rule, Eq. (1.8), we can show that $D > \bar{g}^2/\omega_a$, where D is the coefficient of the A^2 term (see Garziano et al. (2020) for more details). The existence of a lower bound for the value of D is an important issue in the discussion of no-go theorems for the superradiant phase transition, as we discuss in Sect. 1.2.3.

In the limit of weak excitation (linear optical response), we can bozonise the spin operators through the Holstein–Primakoff transformation [Emary & Brandes (2003*b*,*a*)], i.e., $\hat{S}_z \to \hat{b}^\dagger \hat{b} - N/2$, $\hat{S}_+ \equiv \hat{b}^\dagger (N - \hat{b}^\dagger \hat{b})^{1/2}$, and $\hat{S}_- \equiv (N - \hat{b}^\dagger \hat{b})^{1/2} \hat{b}$. In the lowest-order transformation, we get

$$\hat{\mathcal{H}}_v/\hbar \to \omega_c \hat{a}^\dagger \hat{a} + \omega_a \hat{b}^\dagger \hat{b} + \mathrm{i}g(\hat{a}^\dagger + \hat{a})(\hat{b}^\dagger - \hat{b}) + D(\hat{a}^\dagger + \hat{a})^2, \tag{1.16a}$$

$$\hat{\mathcal{H}}_l/\hbar \to \omega_c \hat{a}^\dagger \hat{a} + \omega_a \hat{b}^\dagger \hat{b} + \mathrm{i}\tilde{g}(\hat{a}^\dagger - \hat{a})(\hat{b}^\dagger + \hat{b}) + \frac{\tilde{g}^2}{\omega_c}(\hat{b}^\dagger + \hat{b})^2. \tag{1.16b}$$

By solving the Heisenberg equations of the latter Hamiltonian (length form), we can obtain the resonance frequencies, ω, of the system as

$$\frac{\omega_c{}^2}{\omega^2} = 1 + \frac{4g^2}{\omega_a{}^2 - (\omega + \mathrm{i}0^+)^2}. \tag{1.17}$$

From this, we get two positive ω that correspond to the lower and upper polariton frequencies. As we show in Sect. 1.2.1.3, the second term on the right-hand side corresponds to the optical susceptibility. By replacing 0^+ with a matter damping rate, $\gamma/2$, and ω_c with $\omega_c - \mathrm{i}\kappa/2$ (cavity loss rate κ), we can phenomenologically introduce the effect of dissipation (line broadening).

Note that the two forms of the ISBT Hamiltonian, Eqs. (1.16), are equivalent to each other. They are related through a unitary transformation. Therefore, Eq. (1.17) can also be obtained from Eq. (1.16a), i.e., the Hamiltonian in the velocity form. However, this is possible only if we can set $D = \bar{g}^2/\omega_\mathrm{a}$, i.e., if the oscillator strength is concentrated to the two levels. However, such a truncation procedure cannot be justified in most cases in the velocity form. For more detailed studies of the ISBT Hamiltonian, see a series of papers by Todorov & Sirtori (2012), Todorov (2014), and Todorov & Sirtori (2014).

1.2.1.3 Optical phonons and excitons in bulk semiconductors

In this subsection, we consider optical phonons and excitons in bulk semiconductors that exhibit USC with light [Hopfield (1958), Bamba & Imoto (2016)]. While excitons are not pure bosons, they can be treated as bosons in the weak excitation limit [Combescot et al. (2008)]. In the same manner as in the ISBT case, focusing on just one excitation level, we can express the Hamiltonian in two different forms:

$$\frac{\hat{\mathcal{H}}_v}{\hbar} \approx \sum_{\boldsymbol{k}} \times \left[v|\boldsymbol{k}|\hat{a}^\dagger_{\boldsymbol{k}}\hat{a}_{\boldsymbol{k}} + \omega_{\mathrm{a},\boldsymbol{k}}\hat{b}^\dagger_{\boldsymbol{k}}\hat{b}_{\boldsymbol{k}} + \bar{g}_{\boldsymbol{k}}(\hat{a}^\dagger_{-\boldsymbol{k}} + \hat{a}_{\boldsymbol{k}})(\hat{b}^\dagger_{\boldsymbol{k}} + \hat{b}_{-\boldsymbol{k}}) + D_{\boldsymbol{k}}(\hat{a}^\dagger_{-\boldsymbol{k}} + \hat{a}_{\boldsymbol{k}})(\hat{a}^\dagger_{\boldsymbol{k}} + \hat{a}_{-\boldsymbol{k}}) \right], \tag{1.18a}$$

$$\frac{\hat{\mathcal{H}}_l}{\hbar} \approx \sum_{\boldsymbol{k}} \times \left[v|\boldsymbol{k}|\hat{a}^\dagger_{\boldsymbol{k}}\hat{a}_{\boldsymbol{k}} + \omega_{\mathrm{a},\boldsymbol{k}}\hat{b}^\dagger_{\boldsymbol{k}}\hat{b}_{\boldsymbol{k}} + \mathrm{i}\tilde{g}_{\boldsymbol{k}}(\hat{a}^\dagger_{-\boldsymbol{k}} - \hat{a}_{\boldsymbol{k}})(\hat{b}^\dagger_{\boldsymbol{k}} + \hat{b}_{-\boldsymbol{k}}) + \frac{\tilde{g}_{\boldsymbol{k}}{}^2}{v|\boldsymbol{k}|}(\hat{b}^\dagger_{-\boldsymbol{k}} + \hat{b}_{\boldsymbol{k}})(\hat{b}^\dagger_{\boldsymbol{k}} + \hat{b}_{-\boldsymbol{k}}) \right]. \tag{1.18b}$$

Here, the coupling strengths are defined as $\bar{g}_{\boldsymbol{k}} \equiv [\omega_\mathrm{a}/(v|\boldsymbol{k}|)]^{1/2} g_{\boldsymbol{k}}$ and $\tilde{g}_{\boldsymbol{k}} \equiv (v|\boldsymbol{k}|/\omega_\mathrm{a})^{1/2} g_{\boldsymbol{k}}$ for $g_{\boldsymbol{k}} \equiv \sqrt{\omega_{\mathrm{a},\boldsymbol{k}}\rho/(2\hbar\varepsilon_0\varepsilon_\mathrm{bg})}|\boldsymbol{d}_{1,0}|$ and particle density ρ. The coefficient of the A^2 term satisfies $D_k > \bar{g}_{\boldsymbol{k}}{}^2/\omega_{\mathrm{a},\boldsymbol{k}}$. From the Heisenberg equations (for $D_{\boldsymbol{k}} = \bar{g}^2_{\boldsymbol{k}}/\omega_{\mathrm{a},\boldsymbol{k}}$ in the velocity form), we get the following dispersion relation determining the resonance frequency, ω, as [Hopfield (1958)]

$$\frac{v^2|\boldsymbol{k}|^2}{\omega^2} = 1 + \frac{4g^2}{\omega_{\mathrm{a},\boldsymbol{k}}{}^2 - (\omega + \mathrm{i}0^+)^2}. \tag{1.19}$$

The right-hand side corresponds to the dielectric function divided by ε_bg, and the second term corresponds to the optical susceptibility. We can rewrite its numerator as $4g^2 = f_{1,0}\omega_\mathrm{plasma}{}^2/\varepsilon_\mathrm{bg}$ with the oscillator strength $f_{1,0}$ and the plasma frequency $\omega_\mathrm{plasma} \equiv \sqrt{e^2\rho/(m\varepsilon_0)}$. For a fixed $\boldsymbol{k}$, we can find two positive ω, which correspond to the lower and upper polariton frequencies.

1.2.1.4 Cyclotron resonance (or inter-Landau-level transitions)

In this subsection, we describe CR (or ILLTs) in a 2DEG interacting with cavity photons in the USC regime. We consider the Hamiltonian $\hat{\mathcal{H}}_v$ only in the velocity form, Eq. (1.4), since the calculation is simpler than in the length form. Due to Kohn's theorem [Kohn (1961)], we need not consider the Coulomb interaction $\hat{V}$ for discussing linear optical responses.

We have two separate electromagnetic fields in this problem – (i) a DC magnetic field $\boldsymbol{B}_{\rm DC} = \boldsymbol{\nabla} \times \boldsymbol{A}_{\rm DC}$ represented by a static vector potential $\boldsymbol{A}_{\rm DC}$ and (ii) a dynamical electromagnetic field described by a dynamic vector potential $\boldsymbol{A}(t)$. We include the former contribution to the matter Hamiltonian $\hat{\mathcal{H}}_{\rm mat}$. Then, the matter system is the 2DEG in a DC magnetic field along the z direction as $\hat{\mathcal{H}}_{\rm mat} = \sum_{i=1}^{N} \sum_{\xi=x,y} \hat{\pi}_{i,\xi}{}^2/(2m)$. Here, we defined $\hat{\boldsymbol{\pi}}_i \equiv \hat{\boldsymbol{p}}_i + e\boldsymbol{A}_{\rm DC}$. $N = \rho_{\rm 2DEG} S$ is the total number of electrons, when the surface density of the 2DEG is $\rho_{\rm 2DEG}$.

Introducing the CR frequency $\omega_{\rm cyc} = e|B_{\rm DC}|/m$ and the lowering operator $\hat{c}_i \equiv (\hat{\pi}_{i,y} + {\rm i}\hat{\pi}_{i,x})/\sqrt{2m\hbar\omega_{\rm cyc}}$ between Landau levels (LLs) satisfying $[\hat{c}_i, \hat{c}_j^\dagger] = \delta_{i,j}$ [Yoshioka (2002)], the matter Hamiltonian is rewritten as $\hat{\mathcal{H}}_{\rm mat} = \sum_{i=1}^{N} \hbar\omega_{\rm cyc}(\hat{c}_i^\dagger \hat{c}_i + 1/2)$. Note that CR excitations (i.e., ILLTs) are purely bosonic excitations, and matter levels are not truncated at this stage. Then, the truncation problem does not arise even in the velocity form. In the following, we consider only a bosonic operator $\hat{b} \equiv \sum_{i=1}^{N} \hat{c}_i/\sqrt{N}$ of the collective excitation mode of the 2DEG coherently interacting with the electromagnetic field [Li, Bamba, Zhang, Fallahi, Gardner, Gao, Lou, Yoshioka, Manfra & Kono (2018), Bamba et al. (2019)]. Since the other collective modes are dark (their oscillator strengths are zero) for photons with zero in-plane wavevector, we can truncate such modes, and the matter Hamiltonian is approximated as $\hat{\mathcal{H}}_{\rm mat} \approx \hbar\omega_{\rm cyc}\hat{b}^\dagger\hat{b} + {\rm const.}$

As for photons, for simplicity, we focus on only one cavity resonance frequency $\omega_{\rm c}$ but explicitly consider the two circular polarizations $\xi = \pm$. We define the annihilation operator of the $\pm$ circularly polarized photon as $\hat{a}_\pm \equiv (\hat{a}_x \mp {\rm i}\hat{a}_y)/\sqrt{2}$, where $\hat{a}_{x/y}$ is that of the linearly polarized photon in the x/y direction. Then, when we define the coupling strength as $\bar{g} \equiv (\omega_{\rm cyc}/\omega_{\rm c})^{1/2} g$ and $g \equiv [e^2\rho_{\rm 2DEG}/(2\varepsilon_0\varepsilon_{\rm bg}m)]^{1/2}\psi(z_{\rm 2DEG})$ for the position, $z_{\rm 2DEG}$, of the 2DEG inside the cavity, the total Hamiltonian is obtained from Eq. (1.7a) as

$$\hat{\mathcal{H}}_v \approx \sum_{\xi=\pm} \hbar\omega_{\rm c}\hat{a}_\xi^\dagger\hat{a}_\xi + \hbar\omega_{\rm cyc}\hat{b}^\dagger\hat{b} + {\rm i}\hbar\bar{g}\left[\hat{b}^\dagger(\hat{a}_+ + \hat{a}_-^\dagger) - (\hat{a}_- + \hat{a}_+^\dagger)\hat{b}\right] + \frac{\hbar\bar{g}^2}{\omega_{\rm cyc}}(\hat{a}_- + \hat{a}_+^\dagger)(\hat{a}_+ + \hat{a}_-^\dagger). \tag{1.20}$$

In this way, the CR excitation $\hat{b}$ interacts with the co-circularly polarized photon $\hat{a}_+$ in the co-rotating manner as ${\rm i}\hbar g(\hat{b}^\dagger\hat{a}_+ - \hat{a}_+^\dagger\hat{b})$, while it interacts with the counter-circularly polarized photon $\hat{a}_-$ in the counter-rotating manner as ${\rm i}\hbar g(\hat{b}^\dagger\hat{a}_-^\dagger - \hat{a}_-\hat{b})$.

By solving the Heisenberg equations of motion, the resonance frequencies, $\omega_\pm$, of the coupled modes (polariton modes) with the $\pm$ circular polarization can

be obtained as

$$\frac{{\omega_c}^2}{{\omega_\pm}^2} = 1 - \frac{2g^2}{\omega_\pm(\omega_\pm \mp \omega_{\rm cyc} + {\rm i}0^+)}. \tag{1.21a}$$

More detailed calculations can be found in Li, Bamba, Zhang, Fallahi, Gardner, Gao, Lou, Yoshioka, Manfra & Kono (2018) and Bamba et al. (2019).

1.2.2 Virtual photons and two-mode squeezed vacuum

As pointed out by Ciuti et al. (2005), owing to the presence of the CRTs, the expectation value of the number of photons, $\langle {\rm g}|\hat{a}^\dagger \hat{a}|{\rm g}\rangle$, is nonzero even in the ground state $|{\rm g}\rangle$ in the USC regime. Such photons are called virtual photons. It has been theoretically suggested that the ground state of the light–matter coupled system (polariton system) is expressed as a two-mode squeezed vacuum state of the original photon and excitation modes [Artoni & Birman (1989, 1991), Schwendimann & Quattropani (1992*a*,*b*), Quattropani & Schwendimann (2005)] (a similar discussion has been given for nondispersive dielectric media [Abram (1987), Glauber & Lewenstein (1991)]). Virtual photons (and virtual excitations) compose such an intrinsic squeezed vacuum. The number of virtual photons and degree of squeezing become a considerable value in the USC regime. While the vacuum BS shift [Bloch & Siegert (1940)] has been clearly demonstrated as a hallmark of the CRTs in the CR system by Li, Bamba, Zhang, Fallahi, Gardner, Gao, Lou, Yoshioka, Manfra & Kono (2018), the presence of virtual photons has not yet been proven experimentally. Since the early studies of USC by Ciuti et al. (2005), many proposals for observing virtual photons have been reported.

One of the main strategies is dynamically modulating the coupling strength $g(t)$ or other parameters, by which photons or photon pairs are emitted from the cavity to the outside world [De Liberato et al. (2007), Dodonov et al. (2008), De Liberato et al. (2009), Garziano et al. (2014), Shapiro et al. (2015)]. Such radiation is called quantum vacuum radiation, and the emission process is similar to the dynamical Casimir effect [Moore (1970)]. The modulation frequency should be of the order of the resonance frequencies, and such an experiment has been demonstrated in superconducting circuits [Wilson et al. (2011)].

For more explicit evidence of the presence of virtual photons, one can suddenly turn off the coupling, making g zero. Then, the virtual photons can escape from the cavity, and the correlation functions of those emitted photons should reflect the state of the virtual photons in the ground state [Ashhab & Nori (2010), Auer & Burkard (2012), Garziano et al. (2013), Hagenmüller (2016)]. Such schemes have been proposed for ISBT polaritons [Auer & Burkard (2012)] as well as for Landau polaritons [Hagenmüller (2016)].

As shown in Fig. 1.4(a), spontaneous emission of virtual photons has been proposed by Stassi et al. (2013, 2016) by considering a three-level system embedded in a cavity, which is similar to the ISBT system (two conduction subbands and one valence subband) [Günter et al. (2009)]. When the transition between

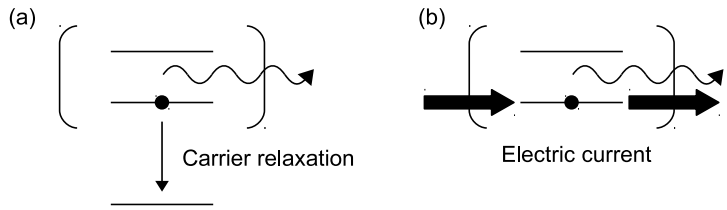

FIGURE 1.4 Sketches of virtual photon emission processes. Virtual photons are released as real photons through (a) spontaneous emission in a three-level system and (b) ground state electroluminescence.

the two excited levels is ultrastrongly coupled with the cavity mode, the virtual photons are emitted by the spontaneous relaxation of the carrier to its most stable level, because the USC diminishes due to the disappearance of the carrier from the above two levels. In a similar system but with driving between the lower two levels (e.g., between a conduction subband and a valence subband), the (stimulated) emission of virtual photons has been proposed [Carusotto et al. (2012), Huang & Law (2014), Stefano et al. (2017)].

Further, in a two-level or two-(sub)band system embedded in a cavity, as shown in Fig. 1.4(b), as carriers pass through just one of the levels or (sub)bands, the emission of photons is expected while the carriers escape from the system (and then the light–matter coupling diminishes). It is called ground state electroluminescence [Cirio et al. (2016, 2019)]. It has also been proposed that the signature of virtual photons can be observed as the Lamb shift of an ancillary probe qubit coupled to the ultrastrongly coupled system [Lolli et al. (2015)]. Further, time-modulated optomechanical coupling has also been proposed by Cirio et al. (2017) for amplifying a mechanical probe of virtual photons.

1.2.3 Superradiant phase transition

Hepp & Lieb (1973) showed that there exists a second-order phase transition in a system of N two-level atoms (with resonance frequency ω_{a}) interacting with a single mode of light (with frequency ω_{c}) described by

$$\hat{\mathcal{H}}_{\mathrm{Dicke}}/\hbar \equiv \omega_{\mathrm{c}}\hat{a}^{\dagger}\hat{a} + \omega_{\mathrm{a}}\left(\hat{S}_z + \frac{N}{2}\right) + \frac{2\bar{g}}{\sqrt{N}}(\hat{a}^{\dagger} + \hat{a})\hat{S}_y. \tag{1.22}$$

Wang & Hioe (1973) also showed the existence of such a phase transition using a different, simpler method. The above Hamiltonian was first used by Dicke (1954) in the context of superradiance, and the predicted phase transition has come to be known as the superradiant phase transition (SRPT) or Dicke phase transition. In the thermodynamic limit ($N \to \infty$), the condition for the superradiant phase to arise is $\bar{g}^2 > \omega_{\mathrm{c}}\omega_{\mathrm{a}}/4$, i.e., the SRPT occurs in the USC regime; see Fig. 1.5. Below a critical temperature, the expectation values of the photon annihilation

operator $\langle \hat{a} \rangle$ and spin operator $\langle \hat{S}_y \rangle$ become finite, signaling a spontaneous appearance of an electromagnetic field and polarization (or electric current) in thermal equilibrium.

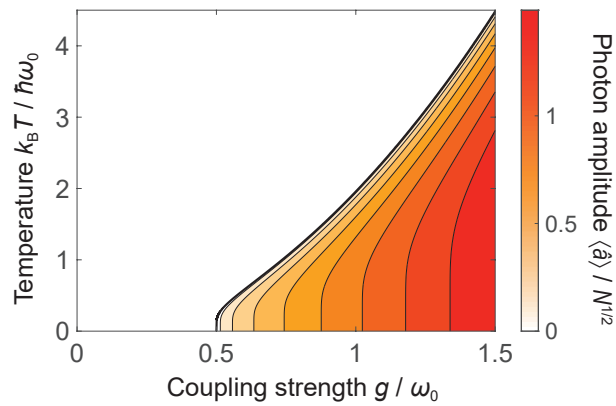

FIGURE 1.5 Phase diagram for the superradiant phase transition predicted by Hepp & Lieb (1973) and Wang & Hioe (1973). The superradiant phase exists in the shaded area, where a finite electromagnetic field and polarization arises in thermal equilibrium.

However, Rzażewski et al. (1975) pointed out that the A^2 term, $D(\hat{a}^\dagger + \hat{a})^2$, is neglected in the above Hamiltonian used by Hepp & Lieb (1973); see, e.g., Eq. (1.14a) for the full Hamiltonian for ISBTs including the A^2 term. Rzażewski et al. (1975) showed that the A^2 term becomes an additional energy cost and prevents the SRPT. In the case of the length form, Eq. (1.14b), it can be shown that the P^2 term (instead of the A^2 term) prevents the SRPT [Yamanoi & Takatsuji (1978)]. The importance of the A^2 or P^2 term in the USC regime has been extensively discussed in relation with the gauge invariance [Woolley (1976), Yamanoi (1976), Yamanoi & Takatsuji (1978), Keeling (2007), Vukics & Domokos (2012), Vukics et al. (2014), Bamba & Ogawa (2014), Vukics et al. (2015), Grießer et al. (2016)]. The influence of gauge choice on the SRPT has also been discussed by Stokes & Nazir (2019*c*).

Through a Bogoliubov transformation, $\hat{a}' \equiv (\hat{a} + \zeta\hat{a}^\dagger)/\sqrt{1-\zeta^2}$, with $\zeta \equiv (\sqrt{1+4D/\omega_c} - 1)/(\sqrt{1+4D/\omega_c} + 1)$, we can eliminate the A^2 term, and thus, Eq. (1.14a) can be transformed to Eq. (1.22), with replacing $\hat{a} \to \hat{a}'$, $\omega_c \to \omega_c' \equiv \sqrt{\omega_c(\omega_c + 4D)}$, $\bar{g} \to \bar{g}' \equiv \sqrt{(1-\zeta)/(1+\zeta)}\bar{g}$. However, $\bar{g}'^2 > \omega_c'\omega_a/4$ cannot be satisfied for $D > \bar{g}^2/\omega_a$, which is obtained by the sum rule, Eq. (1.8). Thus, the presence of the A^2 term itself does not prevent the SRPT, but the minimum magnitude of its coefficient (set by the TRK sum rule) does. A similar calculation can be performed also for the P^2 term.

Starting from the minimal-coupling Hamiltonian $\hat{\mathcal{H}}_v$, Eq. (1.4), without truncation of matter levels nor photonic modes (performed for deriving Eq. (1.22)),

a more general no-go theorem was suggested by Knight et al. (1978) through classical treatment of the electromagnetic fields and polarization. Furthermore, through quantum treatment of the matter but classical treatment of the electromagnetic fields, more general no-go theorems were proposed in the long-wavelength approximation by Bialynicki-Birula & Rzażewski (1979) and in a more general case by Gawędzki & Rzążewski (1981). The classical treatment of the electromagnetic fields can be justified under some conditions, as shown by Bamba & Imoto (2017).

Since the no-go theorem has not yet been completely proven even for the minimal-coupling Hamiltonian, proposals of counterexamples and indications of calculation mistakes have been repeated. For example, longitudinal dipole-dipole interaction [Keeling (2007), Vukics et al. (2014), Bamba & Ogawa (2014), Vukics et al. (2015)], graphene [Hagenmüller & Ciuti (2012), Chirolli et al. (2012)], and the excitonic insulator [Mazza & Georges (2019), Andolina et al. (2019), Nataf et al. (2019)] have been discussed. Currently, the possibility of the SRPT by a short-range depolarizing interaction between atoms proposed by Grießer et al. (2016) has not been denied yet.

In a driven-dissipative situation, a scheme for implementing the Dicke model with $\bar{g} > \omega_c\omega_a/4$ was proposed by Dimer et al. (2007). A SRPT-like transition (a nonequilibrium critical phenomenon) was experimentally demonstrated in cold atoms driven by laser light by Baumann et al. (2010). They were able to tune the coupling strength, $\bar{g}$, by changing the power of the laser light, and the transition was observed by the change in $\bar{g}$. While it was not driven by quantum fluctuations [Larson & Irish (2017)], the transition was called a "quantum" phase transition since the coupling term with the tunable $\bar{g}$ was not commutable with the rest of the Hamiltonian terms. In thermal equilibrium, the SRPT has not been observed. While softening (lowering) of a resonance frequency has been experimentally observed in a CR system by Keller et al. (2020), it remains unclear whether it is a SRPT signature.

As pointed out by Knight et al. (1978), for systems beyond the minimal-coupling Hamiltonian, we can circumvent the above-mentioned no-go theorems even in thermal equilibrium. A SRPT analogue in superconducting circuits has been discussed by Nataf & Ciuti (2010), Viehmann et al. (2011), Ciuti & Nataf (2012), and Jaako et al. (2016), and one proposal by Bamba et al. (2016) has not been repudiated. Further, a 2DEG with Rashba spin-orbit coupling has been proposed by Nataf et al. (2019), which has also not been invalidated. To date, no-go theorems have not been proposed for magnetic materials.

1.2.4 Predictions for materials beyond semiconductors

USC between light and various types of quasiparticles in semiconductors has been demonstrated experimentally, as discussed in detail in Sect. 1.3. In this subsection, we focus on recent theoretical proposals predicting fascinating cavity-enabled phenomena in quantum materials beyond traditional semiconductors. In

particular, some of the recent proposals on cavity control of properties of materials such as superconductors, excitonic insulators, Mott insulators, topological insulators, and other quantum materials are reviewed.

1.2.4.1 Superconductors in cavities

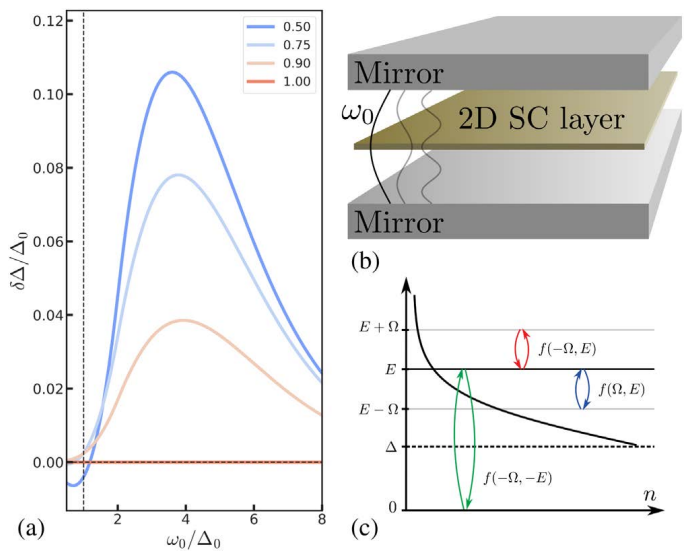

FIGURE 1.6 Enhancement of superconductivity through the cavity quantum Eliashberg mechanism proposed by Curtis et al. (2019). (a) Relative enhancement of the gap function as a function of cavity frequency ω_0. Curves are colored and labeled according to the ratio between the photon and quasiparticle temperatures. Enhancement is seen to set in after the cavity frequency surpasses the pair-breaking energy, $2\Delta_0$. (b) Schematic picture of the system used for the calculation. The lowest cavity resonator mode with cutoff frequency ω_0 is shown, as is the 2D superconducting layer. (c) Depiction of various processes that contribute to the quasiparticle collision integral, plotted against the equilibrium quasiparticle distribution $n(E)$. The blue arrows depict the down-scattering terms captured by $f(\Omega, E)$, the red arrows depict the up-scattering terms captured by $f(-\Omega, E)$, and the green arrows represent the pair processes captured by $f(-\Omega, -E)$.

Superconductivity is one of the fascinating macroscopic manifestations of quantum mechanics. A superconducting state, exhibiting zero resistance and expelling of magnetic fields, occurs below a critical temperature, T_c. There are currently many efforts to control superconducting properties of materials, particularly their T_c. For example, through a static external stimulus such as pressure, the T_c of a material has been raised to 250 K [Drozdov et al. (2019)]. Another approach is based on light illumination, especially utilizing femtosecond laser pulses [see, e.g., Kaiser (2017)]. Nonequilibrium, light-driven superconductivity and Eliashberg enhancement of superconductivity are usually carried out in

free space with an external light source. Light-matter interactions in cavities in the USC regime offer another exciting method for modifying superconductivity properties. There have been several theoretical studies on physical mechanisms affecting superconductivity properties driven by vacuum fluctuations in cavities, as described in the following.

Curtis et al. (2019) studied a 2D BCS superconductor placed in single-mode and multimode cavities. The physical picture is based on the Eliashberg effect [Eliashberg (1970)], i.e., a redistribution of the quasiparticles into a more favorable nonthermal distribution due to an applied electromagnetic field, which was generalized to include both quantum and thermal fluctuations. An enhancement of the superconducting gap by a few percent was predicted; see Fig. 1.6. Cavity Bardasis-Schrieffer mode polaritons and cavity Higgs polaritons were also predicted to exist. The Bardasis-Schrieffer modes are exciton-like states of the superconducting order parameter [Allocca et al. (2019)], while Higgs polaritons are hybridized states between cavity photons and the amplitude mode of a superconductor [Raines et al. (2020)]. Although none of these modes couple linearly to light, they can be observed and controlled by applying a super-current or observed with THz near field techniques [Sun et al. (2020)].

In another study, Sentef et al. (2018) performed Migdal-Eliashberg simulations to explore modifications of electron-phonon interactions arising from the formation of phonon polaritons at the 2D interface of $FeSe/SrTiO_3$. The observed enhancement in the electron-phonon coupling constant, however, did not result in an enhancement of T_c for the forward-scattering pairing mechanism. This negative effect was explained by the quasilinear dependence of T_c on the electron-phonon coupling constant in their model in contrast to BCS exponential scaling. Most recently, there has been an experimental study reporting a 50% increase of T_c in a BCS-type superconductor (Rb_3C_{60}) coupled to surface plasmon polaritons (SPPs) while showing decreasing T_c for $YBa_2Cu_3O_{7-x}$ [Thomas et al. (2019)]. In this study, a powder of superconductors was embedded in a polymer matrix and placed on a gold mirror. Qualitatively, the enhancement of T_c is attributed to cooperative SC between phonons in the superconductor and the surface plasmon polaritons via an auxiliary coupler (polymer).

Schlawin et al. (2019) have predicted superconductivity in a semiconductor 2DEG induced by USC with THz cavity photons. By using realistic parameters of a GaAs 2DEG inside a THz cavity, they predicted that superconductivity with T_c in the low-Kelvin regime should be realized. Virtual photons, in this case, act as the glue for pairing [Schlawin et al. (2019)]. Moreover, in a similar setting, Gao et al. (2020) predicted that driving the cavity might stabilize electron pairing even at higher temperatures. Clearly, cavity QED offers a variety of novel approaches to both manipulation of superconducting materials and investigation of physics behind high-T_c superconductivity.

1.2.4.2 Quantum materials in cavities

As described in Sect. 1.2.3, the Dicke SRPT is one of the most profound collective phenomena in quantum optics. If it is realized in a solid in equilibrium, e.g., a 2DEG [Hagenmüller & Ciuti (2012), Nataf et al. (2019)], it can lead to real-world applications of macroscopic quantum coherence. For so-called *quantum materials*, which host a plethora of collective phases [Tokura et al. (2017)], novel, emergent light-matter collective phenomena have been proposed. Because of the interplay between short-range electrostatic interactions and the nonperturbative coupling to a common cavity mode, several new phases that do not have direct counterparts in the collective Dicke models or solid state spin systems have been shown to exist through numerical calculations by Schuler et al. (2020).

Another example is the superradiant excitonic insulator (SXI), studied by Mazza & Georges (2019). Figure 1.7 shows its phase diagram as a function of the strength of electronic interactions, U, and the light-matter coupling strength, g. The SXI phase is characterized by equilibrium superradiance in the photon field and condensation of excitons in the electronic system happening simultaneously. However, this conclusion is disputed, since the model used by Mazza & Georges (2019) does not guarantee gauge invariance, as pointed out by Andolina et al. (2019) and Nataf et al. (2019).

More recently, Ashida et al. (2020) studied the possibility of observing a SRPT in systems that are naturally close to a spontaneous electric polarization phase. They considered a quantum paraelectric material sandwiched between metallic cladding layers acting as cavity mirrors. In contrast to previous studies, the polariton excitations consist of infrared active phonons in the quantum paraelectric, electromagnetic fields in the cavity, and plasmons in the metallic electrodes. Hence, the enhancement of the ferroelectric phase in quantum paraelectric materials due to cavity-induced optical phonon softening is predicted.

In general, cavities offer novel ways to manipulate and control material properties. In addition to the proposals mentioned above, other examples include manipulation of macroscopic magnetic and electronic properties of strongly correlated electron systems [Kiffner et al. (2019)], nonlinear phononics [Juraschek et al. (2019)], control of excitonic optical spectra of van der Waals materials and heterostructures [Latini et al. (2019)], and QED Chern insulators [Wang et al. (2019)]. Figure 1.8 demonstrates an opening of an energy gap when monolayer graphene is placed into a cavity, predicted by Wang et al. (2019). Here, photon-dressed Dirac fermions show a quantized Hall response with predicted conductance of $2e^2/h$ that can be characterized by an integer Chern number. Overall, the burgeoning field of condensed-matter cavity QED promises the discoveries of new fascinating physics, in addition to those discussed in the next section, paving the way for unprecedented control of material properties.

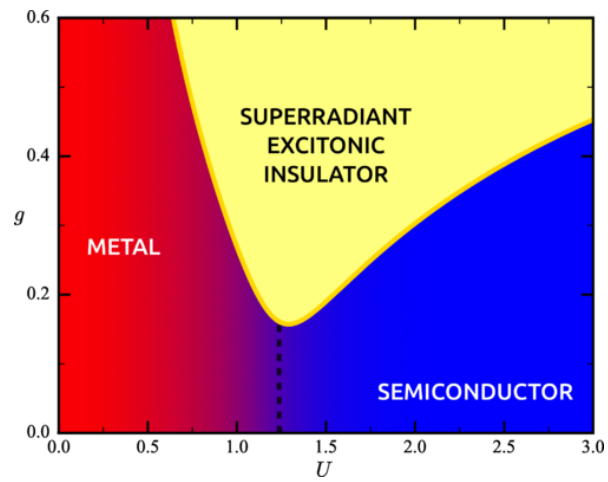

FIGURE 1.7 Phase diagram for interacting electrons strongly coupled with cavity photons proposed by Mazza & Georges (2019). A superradiant excitonic insulator phase exists at certain strengths of electron-electron interactions, U, and light-matter coupling, g. The red and blue intensities reflect band populations. In the metal region (red), both orbitals are occupied, whereas in the semiconductor region (blue) only the valence band is completely filled.

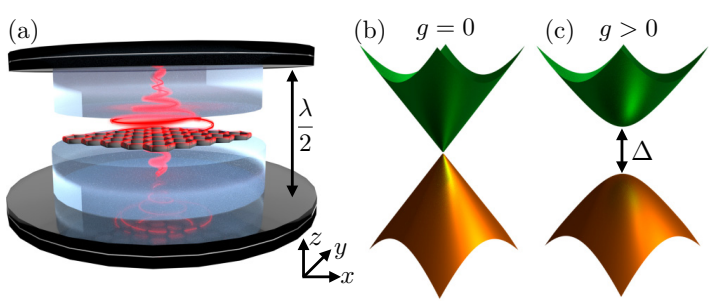

FIGURE 1.8 2D material inside a chiral cavity studied by Wang et al. (2019). (a) Setup for monolayer graphene between cavity mirrors a distance $\lambda/2$ apart, where λ is the wavelength of the fundamental cavity photon mode. The red spiral indicates the circular photon polarization. The 2D material is encapsulated in a dielectric medium (glassy region). (b) Dirac cone of a 2D Dirac material at electron-photon coupling $g = 0$. (c) Energy gap Δ due to time-reversal symmetry breaking for $g > 0$.

1.3 EXPERIMENTAL DEMONSTRATIONS OF ULTRASTRONG COUPLING

Diverse experimental platforms have emerged during the last decade that exhibit USC. These systems include not only traditional light-matter hybrid systems, such as exciton and phonon polaritons in bulk semiconductors, but also intraband transitions (ISBTs and CR), plasmons, phonons, and magnons in low-dimensional systems. In this section, we review some of the pioneering studies as well as the latest experimental observations of USC in these systems.

1.3.1 Intraband transitions

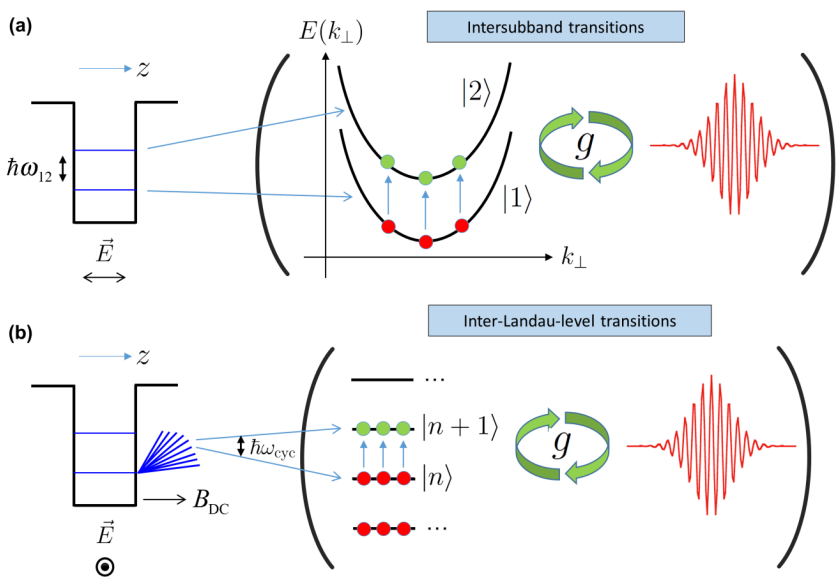

FIGURE 1.9 Cavity polaritons based on intraband transitions in semiconductor quantum wells. (a) ISBTs resonantly coupled at a rate g to a light field $\vec{E}$ polarized along the growth (z) direction. (b) CR, or ILLTs, coupled to a light field $\vec{E}$ polarized in the quantum well (x-y) plane. A DC magnetic field B_{DC} applied along the growth (z) direction quantizes the in-plane (x-y) motion into discrete states (Landau levels) with energy separation $\hbar\omega_{cyc}$.

1.3.1.1 Intersubband-plasmon polaritons

ISBTs, also known as ISB plasmons, are defined as resonant optical transitions between two subbands within the conduction or valence band of a semiconductor QW [see, e.g., Helm (2000) and Paiella (2006)]. They occur at low photon energies, typically in the MIR or THz range, with enourmous dipole moments [West

& Eglash (1985)], which have been advantageously utilized to achieve USC [Dini et al. (2003), Dupont et al. (2003), Anappara et al. (2005, 2006, 2007), Dupont et al. (2007), Sapienza et al. (2007, 2008), Todorov et al. (2009), Anappara et al. (2009), Günter et al. (2009), Geiser et al. (2010), Todorov, Andrews, Colombelli, De Liberato, Ciuti, Klang, Strasser & Sirtori (2010), Zanotto et al. (2010), Jouy et al. (2011), Geiser et al. (2012), Porer et al. (2012), Zanotto et al. (2012), Delteil et al. (2012), Dietze et al. (2013), Askenazi et al. (2014, 2017), Laurent et al. (2017), Jeannin et al. (2019)]. An ISBT is a plasmon excitation because it is a collective response of a 2DEG in the QW to a resonant light field, polarized along the growth (z) direction, with transition frequency $\hbar\omega_{12}$; see Fig. 1.9a. In contrast to interband transitions, whose optical properties are largely determined by the fixed band gap energy of the semiconductor, the use of band-structure engineering provides ISBTs with ample tunability of the transition frequency and oscillator strength, which is of fundamental importance for quantum devices like the quantum cascade laser [Faist et al. (1994)] and the QW infrared photodetector [see, e.g., Choi (1997) and Schneider & Liu (2007)].

Much of the initial work on ISB plasmon microcavity-polaritons in the USC regime (reviewed by Forn-Díaz et al. (2019)) was explored in the MIR range. Todorov et al. (2009) successfully extended the range to the THz band using a metal-dielectric-metal microcavity. This approach, schematically depicted in Fig. 1.10a, realized subwavelength confinement without significant ohmic losses, which led to USC with a large cooperativity value. Figure 1.10b shows low temperature (4.5 K) reflectivity spectra for different values of cavity detuning with respect to the ISBT. A clear anticrossing behavior is observed for the lowest cavity mode ($K = 1$). In Fig. 1.10c the two polaritons branches are plotted as a function of inverse slit-width, $1/s$, which determines $2g/2\pi = 0.8$ THz and $\eta = 0.11$. Todorov, Andrews, Colombelli, De Liberato, Ciuti, Klang, Strasser & Sirtori (2010) further increased the number of QWs to 25 and used a zero-dimensional resonator to go deeper into the USC regime. The photonic structure consisted of square-shaped microcavities formed by an array of metallic pads above and a planar metallic plate below, as shown in Fig. 1.10d. Using this configuration, the authors achieved $2g/2\pi = 1.41$ THz at 4.5 K and a record high value at that time for the normalized coupling strength: $\eta = 0.24$. In addition, it was shown that the polariton splitting exhibited a nonlinear behavior arising from the A^2 term in the light-matter interaction Hamiltonian; see Fig. 1.10e. Finally, the opening of a polaritonic gap of 330 GHz was also observed by plotting the polariton frequencies as a function of cavity frequency; see Fig. 1.10f.

Since 1 THz ~ 4 meV ~ 50 K, THz resonances in two-level (or two-subband) systems are generally observable only at cryogenic temperatures. Geiser et al. (2010) used parabolic QWs, which enables an observation of THz ISBTs even at room temperature since the equally separated energy levels in this multi-level system makes the resonance frequency and strength independent of the electron distribution. The authors placed the QWs in an electronic feedback microcavity resonator consisting of an inductor-capacitor circuit on top and a

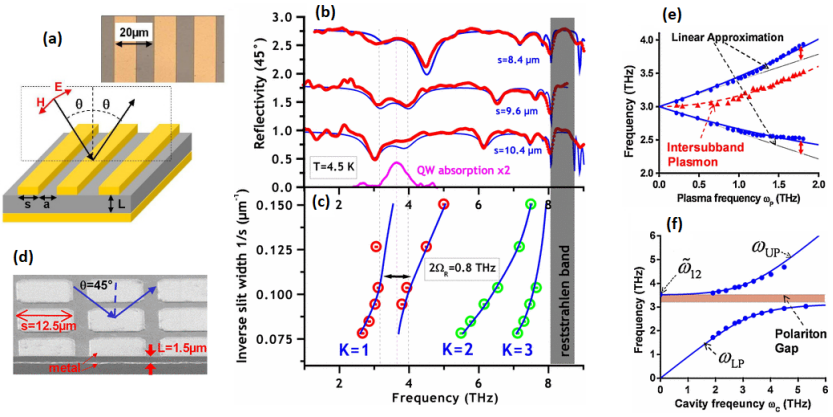

FIGURE 1.10 Intersubband-plasmon polaritons in metal-dielectric microcavities in the USC regime at terahertz frequencies. (a) Schematic of the photonic structure used by Todorov et al. (2009). Top: top view of the metallic lamellar grating. Bottom: schematic of the geometry used for reflectivity measurements and side view of the grating. (b) Reflectivity spectra at 4.5 K for different values of the strip width parameter s. (c) Polariton branches plotted as a function of inverse slit-width, $1/s$. The lowest cavity mode ($K = 1$) shows an anticrossing behavior with the ISBT. (d) Electron microscopy image of the metal-dielectric-metal photonic structure used by Todorov, Andrews, Colombelli, De Liberato, Ciuti, Klang, Strasser & Sirtori (2010). (e) LP and UP peaks (blue dots) plotted as a function of the plasma frequency. The ISB plasmon energy is also plotted (red triangles). Deviations from the linear approximation are clearly observed. (f) Polariton resonances plotted as a function of cavity frequency. The opening of a polaritonic gap is seen. Adapted from Todorov et al. (2009), Todorov, Andrews, Colombelli, De Liberato, Ciuti, Klang, Strasser & Sirtori (2010), and Todorov, Tosetto, Teissier, Andrews, Klang, Colombelli, Sagnes, Strasser & Sirtori (2010).

gold ground plane below; see Fig. 1.11a. The cavity mode frequency was tuned by varying the wire (i.e., inductor) length that connects the circular capacitive elements. Figure 1.11b shows an anticrossing curve at 300 K, together with an ISBT spectrum (inset) and energy (horizontal gray line). The observed Rabi splitting, $2g/2\pi = 0.96$ THz, corresponded to $\eta = 0.14$. Importantly, these results were shown to be temperature-independent in the 10 K – 300 K range.

Furthermore, Geiser et al. (2012) studied the role of electron-electron interactions in the USC regime. In a parabolic QW, due to Kohn's theorem [Kohn (1961), Brey et al. (1989)], the depolarization field is not expected to be a limiting factor for η, since its effect is compensated by strong electron-electron interactions. For a highly doped sample, the authors obtained $2g/2\pi = 2.4$ THz, corresponding to $\eta = g/\tilde{\omega} = 0.27$; see Fig. 1.11c. Here, $\tilde{\omega}$ is the ISB plasmon frequency, including electron-electron interaction effects. The authors used both a single-particle model and an interacting electron model [Todorov, Andrews, Colombelli, De Liberato, Ciuti, Klang, Strasser & Sirtori (2010), Ciuti et al. (2005)] (see Fig. 1.11d) to fit the polariton frequencies. It was shown that even though the different electron-electron interactions cancel out each other as a consequence of Kohn's theorem and lead to $\tilde{\omega} = \omega_{12}$, the plasma frequency remains an important physical quantity in the USC regime, explaining the opening of a polaritonic gap.

1.3.1.2 Landau polaritons (or cyclotron resonance polaritons)

A magnetic field applied in the growth (z) direction of a QW leads to the quantization of the electronic orbital motion into a ladder of equally separated LLs with a spacing $\hbar\omega_{\mathrm{cyc}} = eB_{\mathrm{DC}}/m^*$, where e is the electronic charge, B_{DC} is the applied external magnetic field, and m^* is the effective carrier mass (see Fig. 1.9b) [see, e.g., Lax & Mavroides (1960), McCombe & Wagner (1975), Kono (2001), Hilton et al. (2012)]. To couple with the optical transition between the highest occupied and lowest unoccupied Landau levels, the THz electric field polarization must be in the QW plane. From an experimental point of view, realizing ILLTs is easier than ISBTs because normal incidence transmission measurements can be made. In addition, since the resonance frequency of ILLTs linearly depends on B_{DC}, ample tunability of the transition frequency for the matter subsystem can be achieved. In this subsection, we discuss some of the seminal and most recent experimental studies in this field [Muravev et al. (2011), Scalari et al. (2012, 2013), Muravev et al. (2013), Maissen et al. (2014), Zhang, Lou, Li, Reno, Pan, Watson, Manfra & Kono (2016), Abdurakhimov et al. (2016), Maissen et al. (2017), Bayer et al. (2017), Keller et al. (2017), Paravicini-Bagliani et al. (2017, 2018), Li, Bamba, Zhang, Fallahi, Gardner, Gao, Lou, Yoshioka, Manfra & Kono (2018), Keller et al. (2018), Rajabali et al. (2019), Keller et al. (2020)].

Muravev et al. (2011) observed cavity polaritons in an AlGaAs/GaAs QW structure using coplanar microresonators. These hybrid modes arose from the

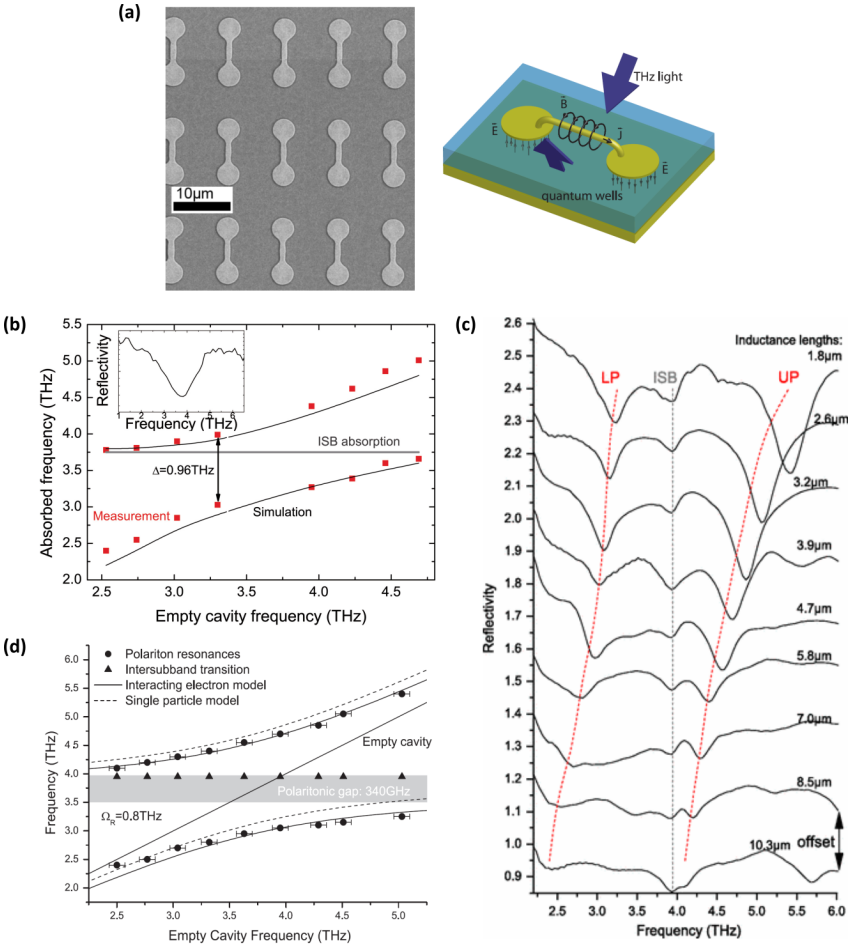

FIGURE 1.11 Intersubband plasmon polaritions in the USC regime at room temperature and terahertz frequencies using parabolic semiconductor QWs studied by Geiser et al. (2010) and Geiser et al. (2012). (a) Left: scanning electron microscopy image of the cavity showing an array of inductor-capacitor resonators. Right: schematic of the electronic microcavity coupled to the semiconductor QWs. (b) Anticrossing curve at 300 K. The frequencies of the reflection minima (red squares) are plotted as a function of cavity frequency. Inset: ISB absorption spectrum at 300 K. (c) Reflection spectra from samples with different inductive lengths. The LP and UP branches as well as the ISB absorption are indicated. (d) Polariton resonances (black dots) as a function of bare cavity frequency, showing the opening of a polaritonic gap (grey shaded area). Solid and dashed lines are a fit to experimental data using single-particle and interacting electron models, respectively. The empty cavity frequency line and the ISB absorption (black triangles) are also indicated. Adapted from Geiser et al. (2010) and Geiser et al. (2012).

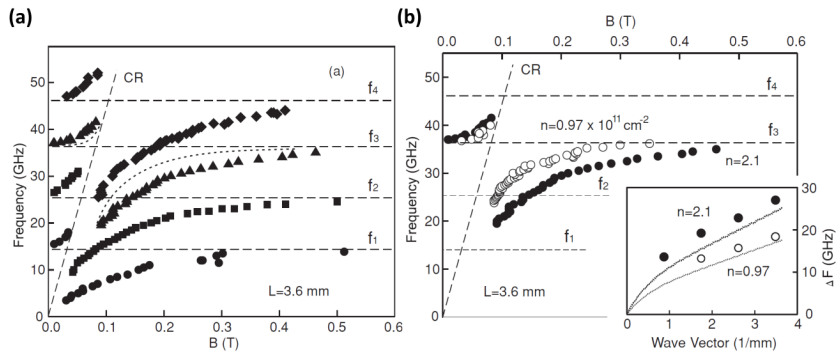

FIGURE 1.12 Hybrid plasmon-photon modes in the microwave transmission of coplanar resonators. (a) Observed anticrossing behavior between the photon modes of the microresonator (f_N, $N = 1, 2, ...$) and the magnetoplasmon resonance (CR). Different symbols correspond to different polariton modes. (b) Electron density (n) dependence of the third polariton mode's anticrossing. Curves can be seen shifting closer to the photon dispersion line when the electron density is decreased. Inset: VRS (denoted as ΔF here) as a function of polariton wavevector for two values of n. Dashed lines are theoretical results. Adapted from Muravev et al. (2011).

USC between magnetoplasmons (CR) in the 2DEG system and the photon modes of the microresonator. By placing the sample in a helium cryostat at the center of a superconducting solenoid and performing microwave transmission measurements as a function of B_{DC}, the authors were able to resolve both of the magnetodispersion branches; see Fig. 1.12a. In addition, the advantages of working with ILLTs was experimentally demonstrated as well, where by changing the electron density or applying an external magnetic field the authors showed how both the Rabi frequency and the dispersion of the cavity polaritons can be tuned over a wide range of frequencies; see Fig. 1.12b.

Zhang, Lou, Li, Reno, Pan, Watson, Manfra & Kono (2016) studied a high-mobility 2DEG placed at the center of a high-Q 1D photonic crystal cavity (PCC) using THz magnetospectroscopy. The maximum value of the electric field was located at the 2DEG position inside the cavity. The 1D PCC was fabricated using a series of alternating dielectric materials with a large refraction index contrast in the THz range. For this work, the authors used vacuum and Si slabs as the low and high index of refraction materials, respectively. The contrast in their indices reduced the number of layers needed to achieve a high-Q cavity to just four [Yee & Sherwin (2009), Chen, Liu, Liu & Hong (2014)]. The authors simultaneously achieved high values of cooperativity and coupling strength, putting the system in the USC regime with $\eta \sim 0.1$, $C > 300$, and $Q \sim 10^3$. This unique combination of parameters allowed the experimental observation of Rabi oscillations in the time-domain traces, persistence of an ultrastrongly

coupled state even when the detuning was off-resonant (see Fig. 1.13a,b), a $\sqrt{n}$ dependence of the VRS with the electron density, n, and a suppression of the superradiant decay of CR [Zhang, Lou, Li, Reno, Pan, Watson, Manfra & Kono (2016), Zhang, Arikawa, Kato, Reno, Pan, Watson, Manfra, Zudov, Tokman, Erukhimova, Belyanin & Kono (2014)].

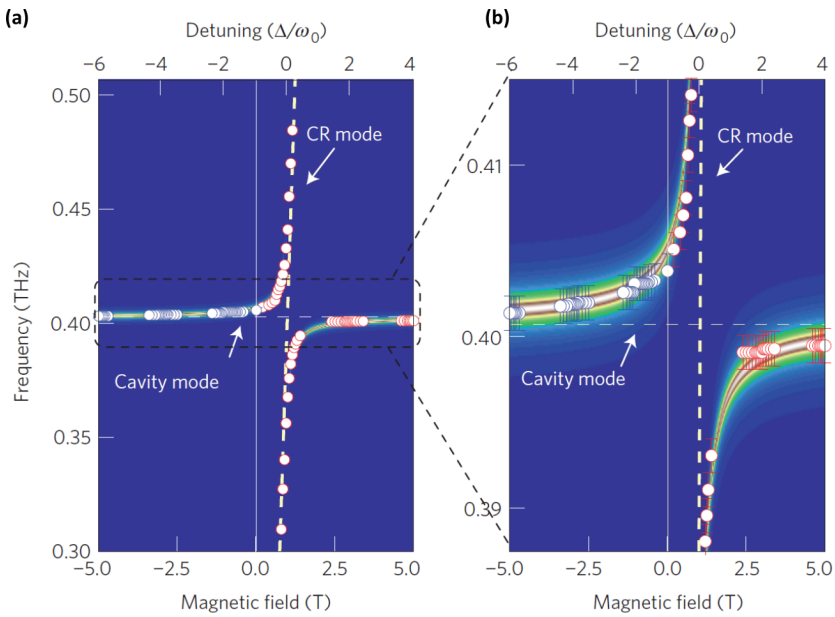

FIGURE 1.13 Cooperative USC of the ILLT of 2D electrons with photons in a high-Q THz cavity. (a) LP and UP branches observed in the vicinity of the anticrossing region. The applied DC magnetic field tunes the cyclotron frequency ω_{cyc} with respect to the (fixed) cavity mode frequency, ω_0. Open circles are experimental data and color lines are THz transmission spectra obtained from electromagnetic field simulations. (b) Zoom-in of the dashed area shown in (a). Deviations from the cold cavity frequency limit persist at negative magnetic fields and can be observed even for a large off-resonant detuning. Adapted from Zhang, Lou, Li, Reno, Pan, Watson, Manfra & Kono (2016).

Paravicini-Bagliani et al. (2018) studied magnetotransport properties of a 2DEG coupled to a subwavelength electronic resonator in the USC regime. The authors prepared two samples with different coupling strengths and resonant frequencies ($\eta = 0.2$ and 0.3 and $\omega_0 = 205$ GHz and 140 GHz, respectively) both of which consisted of a Hall bar placed in the capacitive gap of a complementary LC resonator; see Fig. 1.14a. The current was along the source-drain channel (parallel to the x-axis direction, see Fig. 1.14b), and the longitudinal resistivity, ρ_{xx}, was measured, as indicated in Fig. 1.14a. A significant reduction of the amplitude of the Shubnikov-de Haas oscillations was observed (see Fig. 1.14c), which was theoretically shown to arise from the strong interaction with the

cavity's vacuum field fluctuations [Bartolo & Ciuti (2018)]. In addition, the authors measured the irradiation-induced change in ρ_{xx} by illuminating the sample with a single-frequency, tunable, subterahertz source. The changes observed in ρ_{xx} were strongly dependent on whether the filling factor, ν, was an integer or half-integer; see Fig. 1.14d.

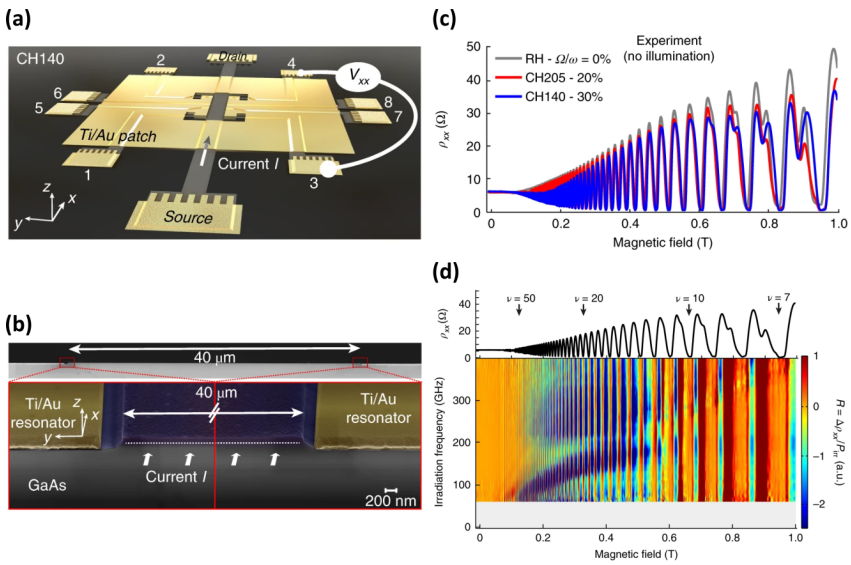

FIGURE 1.14 Magnetotransport in a 2DEG controlled by THz cavity photons. (a) Sample: a Hall bar (center, grey) placed in the capacitive gap of a subwavelength LC resonator (gold structure). (b) SEM image showing a y-z cut of the Hall bar and the Ti/Au electronic resonator. (c) Shubnikov-de Haas oscillations for three samples (η = 0, 0.2, and 0.3, respectively) showing a reduction of the modulation amplitude as the coupling strength is increased. (d) Longitudinal resistance change $\Delta\rho_{xx} = \rho_{xx}^{\text{illu}} - \rho_{xx}^{\text{dark}}$ when illuminated with a narrow-band subterahertz source normalized to the irradiation power P_{irr}. Strong dependence on the spectrum with the filling factor, ν, is observed. Adapted from Paravicini-Bagliani et al. (2018).

Keller et al. (2020) studied Landau polaritons in highly nonparabolic 2DEGs in the USC regime. The authors used InSb QWs and strained Ge QWs with a nonparabolic heavy-hole band. The CR of the 2D electron or hole gas was coupled to a THz metamaterial resonator that presented subwavelength confinement of the electric field; see Fig. 1.15a. By increasing the coupling strength via lithographical adjustment of the cavity mode to lower frequencies, the authors were able to observe significant deviations from the standard Hopfield model and a more consistent agreement of the data with a Hopfield model that had a reduced diamagnetic term (A^2 term); see Fig. 1.15b. Possible explanations of the observed behavior include strain, spin-orbit coupling effects, nonparabolic band dispersions, and the enhanced magnetic coupling in the system that arises from

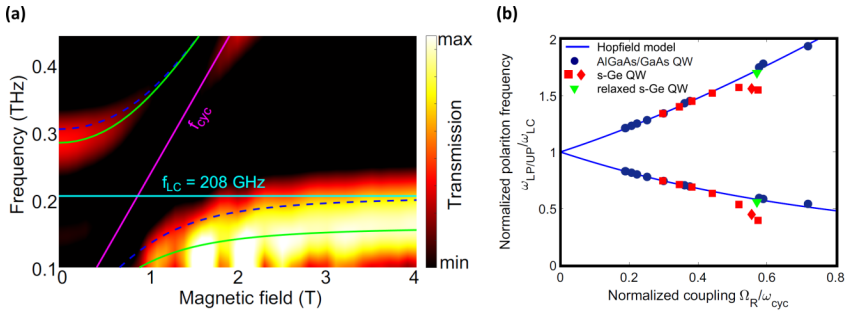

FIGURE 1.15 Landau polaritons in nonparabolic 2DEGs in the USC regime. (a) THz transmission of a strained Ge QW at high filling factors as a function of B_{DC} at 3 K. Solid cyan and magenta lines indicate the cavity frequency and CR of the QW, respectively. The polariton dispersions are fit using a Hopfield model with a reduced diamagnetic (or A^2) term (solid green lines) and without it (solid blue lines). As B_{DC} increases and the CR becomes far-detuned, the cold cavity frequency limit is not recovered, and a LP gap opening is observed. (b) Normalized UP and LP frequencies at the position of minimal splitting plotted as a function of η. Solid blue lines indicate predictions by the Hopfield model, which agree with the experimental results for the standard GaAs QWs and a strain-relaxed Ge QW sample. Deviation from this model are seen for the strained Ge QWs as η increases. Adapted from Keller et al. (2020).

the subwavelength electric field confinement. An open question from this work is whether this method can be extended and used to realize the Dicke SRPT in thermal equilibrium, which is expected to occur when the lower polariton branch becomes gapless.

1.3.2 Plasmon-phonon polaritons

The coupling of collective motion of conduction electrons driven by external electromagnetic waves and lattice vibrations results in a hybrid polariton, which is a mixture of a plasmon polariton and a phonon polariton. Such *plasmon-phonon polaritons* were first identified in doped bulk polar semiconductors as a hybrid of longitudinal optical (LO) phonons and bulk plasmons. Later, the advent of nanomaterials and nanophotonics has enabled confinement and manipulation of light to dimensions much smaller than the wavelength of light, i.e., beyond the diffraction limit. This has made plasmon-phonon polaritons tunable and low-loss nano-objects useful for MIR and THz technology. Furthermore, ingenious designs of nanophotonic cavities have pushed the coupling strength into the USC regime, which has opened up new opportunities for plasmon-phonon polaritons, such as control of chemical reactivity and quantum metrology with high-resolution spectroscopy.

This subsection is organized as follows: a brief historical review of LO phonon-plasmon coupling in doped polar semiconductors is presented, followed

by several exciting examples of the coupling between SPPs and surface phonon polaritons (SPhPs), which is uniquely manifested in nanophotonic structures and nanomaterials. Finally, efforts to enhance the coupling strength into the USC regime are reviewed.

1.3.2.1 Plasmon-phonon polaritons in bulk semiconductors

Polar semiconductors, such as GaAs, AlAs, and InAs, display a narrow high-reflectivity spectral range that is referred to as the Reststrahlen band. This range is bounded by the transverse optical (TO) and LO phonons, whose quantitative expression is characterized through the Lyddane-Sachs-Teller relation (Fig. 1.16a) [Caldwell et al. (2015)]. As the free carrier concentration of these semiconductors increases, the plasma frequency shifts toward higher frequencies, approaching the LO phonon frequency. This causes a spectral blueshift and a shallower slope of the LO phonon edge of the Reststrahlen band. The dielectric function, $\varepsilon(\omega)$, is then modified through the addition of a Drude term describing free carriers to the Lorentz term describing the TO phonon resonance. The eigenfrequencies of supported longitudinal modes are the solutions to the equation $\varepsilon(\omega) = 0$, and instead of a single LO phonon frequency, there are now two solutions signaling the hybridization of plasmons and phonons. The theory of plasmon-phonon polaritons [Yokota (1961), Varga (1965), Singwi & Tosi (1966)] was verified in Raman scattering experiments of bulk doped GaAs [Mooradian & Wright (1966), Mooradian & McWhorter (1967)]. Mooradian & Wright (1966) provided a clear experimental demonstration of these coupled modes, where anticrossing behavior of Raman lines was observed (Fig. 1.16b). Similar avoid crossing behaviors were also observed in infrared reflectivity measurements [Olson & Lynch (1969), Kukharskii (1973), Perkowitz & Thorland (1975), Gaur (1976), Chandrasekhar & Ramdas (1980)] and many other doped bulk polar semiconductors, such as AlGaAs [Kim & Spitzer (1979)], SiC [Klein et al. (1972), Harima et al. (1995), Chafai et al. (2001)], CdTe [Perkowitz & Thorland (1975)], GaN [Kozawa et al. (1994)], InP [Artús et al. (1999)], InSb [Gaur (1976)], and InAs [Gaur (1976), Hasselbeck et al. (2002)].

1.3.2.2 Surface plasmon-phonon polaritons

The advent of nanophotonics has created a new playground for exploring light-matter interactions at the nanoscale. Manipulation of light beyond the diffraction limit has been the persistent focus of nanophotonics, where photons can strongly couple with either plasmons (SPPs) or phonons (SPhPs) [Caldwell et al. (2016)]. Initial research started with SPPs in metals, including Au, Ag, and Al in the ultraviolet to the near-infrared, which has recently been extended to the MIR and THz using alternative plasmonic materials by Hoffman et al. (2007). Doped semiconductors are attractive because of their ability to tune the spectral range of resonance frequency [Law et al. (2012), Sachet et al. (2015), Zhong et al. (2015)]. In this regard, graphene arguably has the most dynamic and tunable range, while

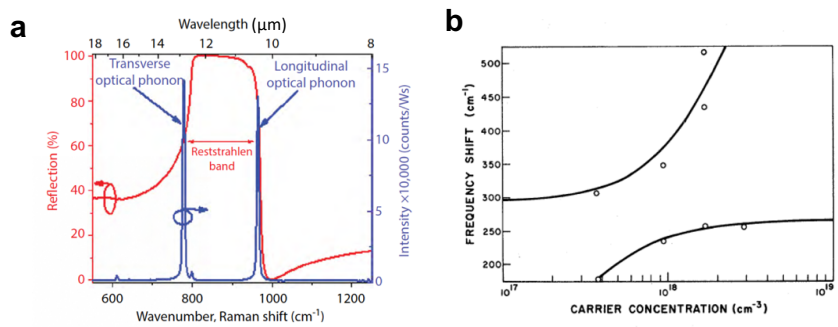

FIGURE 1.16 The Reststrahlen band and manifestations of LO phonon-plasmon coupling in doped bulk semiconductors. (a) Reflectivity (red trace) and Raman (blue trace) spectra of SiC obtained by Caldwell et al. (2015). (b) Anticrossing in Raman scattering of GaAs observed by Mooradian & Wright (1966).

possessing extreme optical confinement of SPPs [Jablan et al. (2009), Ju et al. (2011), Koppens et al. (2011), Grigorenko et al. (2012), Gao et al. (2012), Chen et al. (2012), Fei et al. (2012), Gao et al. (2013, 2014)]. However, these materials suffer from short lifetimes (10s of fs) and propagation distances, and broad resonance features [Khurgin (2015)], limiting their deployment for applications.

On the other hand, SPhPs supported in dielectric polar crystals are promising alternatives with long lifetimes (10s of ps). Candidate materials include polar semiconductors, such as SiC and InP, and polar insulators, such as hexagonal boron nitride (hBN) and SiO_2, with their Reststrahlen bands in the MIR and THz. Their nanostructures thus exhibit much sharper resonance features (with Q factors 10s and 100s) [Wang et al. (2013), Chen, Francescato, Caldwell, Giannini, Maß, Glembocki, Bezares, Taubner, Kasica, Hong et al. (2014), Caldwell et al. (2014), Autore et al. (2018)], compared to those in SPP resonators (with $Q < 10$). Graphene nanoribbons have been demonstrated to support strong localized plasmon resonances, whose frequencies can be broadly tuned (Fig. 1.17a) [Ju et al. (2011)]. Nanoribbons made of hBN sheets can instead support strong SPhPs in its Reststrahlen band; see Fig. 1.17b. As a comparison, the experimental Q of hBN ribbons is ≈ 70 while graphene ribbons have $Q \approx 1 - 2$. Despite the benefits of low loss, propagating SPhPs still have short propagation distances mainly due to the slow velocities [Caldwell et al. (2015), Yoxall et al. (2015)], and the operation frequency window is limited to a narrow range. Coupled SPPs and SPhPs thus can provide a platform with advantages of individual constituents, if two materials are judiciously combined with sufficient spectral, spatial, and mode symmetry overlap, which will lead to broadband, tunable, and long-lifetime polaritons for MIR and THz optics.

Among many demonstrations of the hybrid materials combination, the cou-

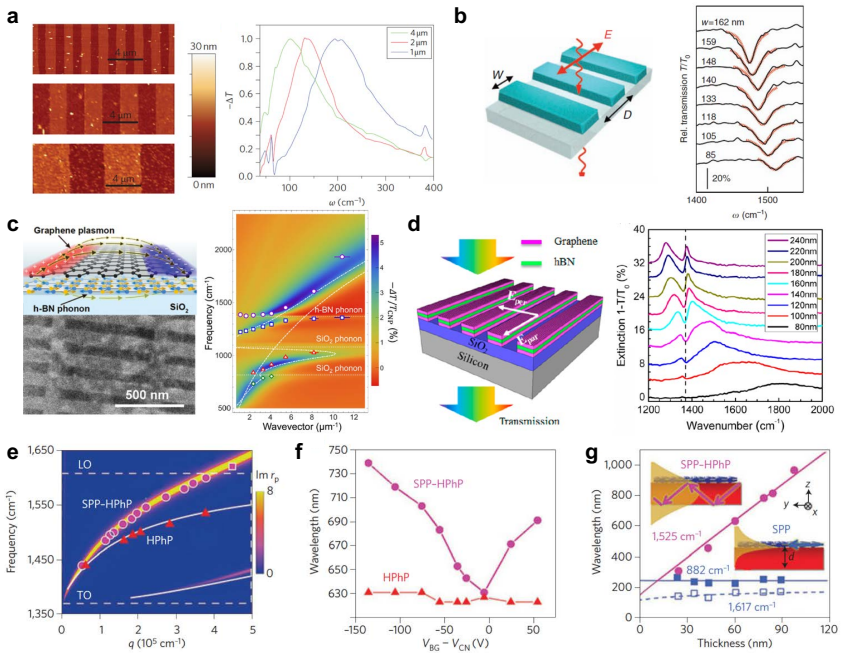

FIGURE 1.17 SPPs and SPhP nanoresonators in graphene and hBN. (a) Graphene ribbons and electric gating to change the Fermi level. Infrared spectra of graphene ribbons with varying widths. Adapted from Ju et al. (2011). (b) hBN ribbons and infrared spectra of ribbons with different widths. Adapted from Autore et al. (2018). (c) Graphene/hBN nanoribbons together with their calculated (white dashed lines) and experimental dispersion (colored markers). Adapted from Brar et al. (2014). (d) Multilayer graphene/hBN ribbons and their infrared spectra. Adapted from Jia et al. (2015). (e) Calculated and corresponding experimental dispersion relationship of the hybridized graphene SPPs and hBN SPhPs (pink circles and square) and pure hBN (red triangles), which is visualized in terms of the imaginary part of the reflection coefficient. (f) Dependence of the polariton wavelength on the applied bias, with respect to the charge neutrality point, of graphene within the graphene/hBN (pink circles) and hBN (red triangles). (g) hBN thickness dependence of polariton wavelength for coupled SPP-HPhPs within graphene/hBN at 1525 cm^{-1} (pink circles), and of graphene SPP modes at 882 and 1617 cm^{-1} (filled and open blue squares, respectively). Schematics of the SPP-HPhP and SPP modes are provided as insets with graphene represented by the blue top layer and hBN by the red slab with thickness. Adapted from Dai et al. (2015) and Caldwell et al. (2016).

pling of SPPs in graphene with SPhPs in hBN has attracted much interest [see, e.g., Brar et al. (2014) and Dai et al. (2015)]. Especially SPhPs supported in thin layers of hBN are hyperbolic phonon polaritons (HPhPs), where hyperbolicity is defined as an extreme birefringence with permittivities along orthogonal crystal axes possessing opposite signs. Hyperbolic polaritons allow electromagnetic modes with large momenta to propagate within the Reststrahlen band [Poddubny et al. (2013), Ferrari et al. (2015)]. Brar et al. (2014) reported hybrid SPP-SPhP polaritons in coupled graphene and hBN ribbons. The dispersion relations of the coupled graphene SPPs/h-BN SPhPs were derived from measurements of nanoresonators with varying widths, where the graphene SPP mode exhibits an anticrossing behavior near the energy of the hBN optical phonon; see Fig. 1.17c. Later, Jia et al. (2015) engineered the coupling by varying the hBN thickness in a layer-by-layer manner (Fig. 1.17d). A systematic experimental study of this coupling using scanning near-field optical microscopy revealed the dispersion relation of SPP-HPhP in graphene/hBN heterostructures and pure HPhP in hBN; see Fig. 1.17e. The polariton wavelength within graphene/hBN heterostructures could be varied by > 20% compared with hBN, by changing the free carrier density in graphene (Fig. 1.17f), and it is also sensitive to the thickness of hBN (Fig. 1.17g pink line) while SPP waves in graphene were independent of thickness (Fig. 1.17g blue lines).

1.3.2.3 Ultrastrong coupling of SPP and SPhP

Despite much success in understanding and demonstrating the physics of plasmon-phonon polaritons in a variety of materials, the coupling strength has remained quite limited due to the intrinsically weaker oscillator strengths of vibrational modes compared to electronic transitions. In addition, the SPP waves are more weakly bonded to the surface at long wavelengths, leading to a significantly higher mode volume. Although engineering phonon properties in materials can be challenging, nanophotonic tools have enabled ingenious design of structures possessing ultrasmall mode volumes, which can greatly enhance light-matter interaction strengths.

Very recently, Yoo et al. (2020) utilized the epsilon-near-zero (ENZ) properties of coaxial nanocavities possessing extreme light confinement in a few-nm gap to achieve USC of vibrational modes in SiO_2. The designed cavities exhibited a transmission resonance that can be understood as either an ENZ resonance or a zeroth-order FP resonance, and the resonance frequency can be shifted by adjusting geometric parameters while maintaining strong optical confinement (Fig. 1.18a). As the resonance happens near the frequency where the dielectric constant is close to zero, the electric field is approximately spatially uniform with a very long effective wavelength to collectively connect a wide range of oscillators for boosting the coupling strength. Thus, as the dimension of the designed cavities is continuously changed and the resonance frequency is swept across the SiO_2 LO phonons, a clear anticrossing in transmission spectra is ob-

served (Fig. 1.18b) and detailed analysis reveals that the Rabi splitting is 50 % of the resonance frequency, or $\eta \sim 0.25$.

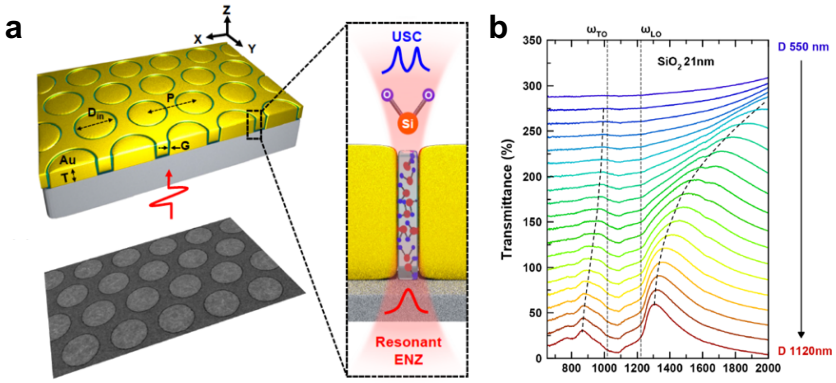

FIGURE 1.18 Ultrastrong plasmon-phonon coupling in the MIR. (a) Schematics and scanning electron microscope images of coaxial nanocavities filled with SiO_2. (b) Infrared transmission spectra of coaxial nanocavities filled with SiO_2 of varying diameters. Adapted from Yoo et al. (2020)

.

1.3.3 Exciton polaritons

Excitons resonantly interacting with photons in a microcavity – microcavity exciton polaritons – have been studied for many years since the pioneering work on GaAs QWs by Weisbuch et al. (1992). GaAs QWs are sandwiched between two epitaxially grown distributed Bragg reflectors (DBRs) that form a cavity [Weisbuch et al. (1992), Bloch et al. (1998), Skolnick et al. (1998), Deng et al. (2002)]. The formed cavity can display a sharp resonance in reflectivity, and the electric or magnetic field can be maximized at the position where QWs are located. When the exciton energy is on resonance with a cavity mode frequency, two dips or peaks appear in a reflectivity or transmittance spectrum with a clear anticrossing behavior. However, the oscillator strength of Wannier excitons in GaAs QWs is typically small, leading to small η, typically less than 10^{-3}. Furthermore, the exciton binding energy is comparable to the ambient thermal fluctuations, and thus, the strong coupling limit, $C > 1$, is achieved only at cryogenic temperatures. Wannier excitons in other inorganic semiconductors, including GaN [Christmann et al. (2008)] and ZnO [van Vugt et al. (2006), Chen et al. (2011), Guillet et al. (2011)], with larger exciton binding energies and oscillator strengths, have been utilized to push the operation temperature to room temperature and achieve larger values of η, but USC has never been

obtained for excitons in inorganic semiconductors.

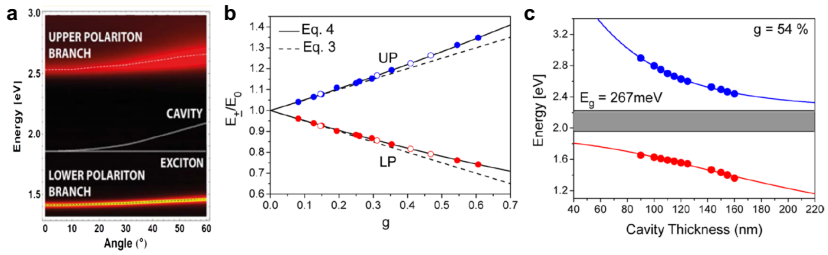

FIGURE 1.19 Ultrastrong coupling of excitons and photons in organic semiconductor squaraine in a microcavity. (a) Contour plots of angle-resolved transmission spectra for a 140-nm-thick microcavity entirely filled with squaraine. (b) Polariton peak energies of UPs and LPs normalized to the transition energy as a function of coupling strength. Both solid and empty dots are from experiments. Dashed lines are calculated eigenfrequencies of the approximated Hamiltonian ignoring CRTs, while solid lines are calculated eigenfrequencies of the full Hamiltonian. (c) Polariton peak energies as a function of cavity thickness (detuning) at $\eta = 0.54$. Solid dots are experimental data and solid lines are calculation based on the Hopfield Hamiltonian. Shaded area indicates a polariton gap. Adapted from Gambino et al. (2014).

Screening is typically weak in organic materials because of their small dielectric constants, which leads to the formation of Frenkel excitons with Bohr radii of the same order as the size of the unit cell. These excitons possess large binding energies and oscillator strengths and generally display, when in cavities, larger values of η than Wannier excitons. Some exemplary materials include tetra-(2,6-t-butyl)phenol-porphyrin zinc (4TBPPZn) ($\eta \approx 0.03$) [Lidzey et al. (1998)], J aggregates ($\eta \approx 0.09$) [Wei et al. (2013)], 2,7-bis[9,9-di(4-methylphenyl)-fluoren-2-yl]-9,9-di (4-methylphenyl)fluorene ($\eta \approx 0.14$) [Kéna-Cohen & Forrest (2010)], and squaraine ($\eta \approx 0.27$) [Gambino et al. (2014)]. Figure 1.19a displays angle-dependent transmission measurements with TE polarized light for the full cavity containing squaraine (contour plot) and a bare cavity (circular dots). Both the upper and lower polariton branches display an almost dispersionless behavior and agree with theoretical results based on the transfer matrix method, which intrinsically takes into account the CRTs. Figure 1.19b shows the upper and lower polariton energies normalized to the exciton energy as a function of coupling strength. Linear relation is only approximately valid if $\eta < 0.2$, while large deviation from linear dependence when $\eta > 0.2$ can be excellently corrected using the full Hopfield model, suggesting that USC is achieved. Also, a polariton gap is observed in the dispersion for a system with $\eta = 0.54$, which is another evidence of USC (see Figure 1.19c).

Emerging nanomaterials, such as semiconducting single-wall carbon nanotubes (SWCNTs) [Graf et al. (2016, 2017), Gao et al. (2018)], transition metal

dichalcogenides (TMDs) [Liu et al. (2015), Dufferwiel et al. (2015), Liu et al. (2016), Chen et al. (2017), Lee et al. (2017), Dufferwiel et al. (2017), Sun et al. (2017)], and low-dimensional perovskites [Su et al. (2017), Wang et al. (2018), Zhang et al. (2018), Shang et al. (2018), Su et al. (2018), Bao et al. (2019), Su et al. (2020)], have characteristics of both Wannier and Frenkel excitons, where the exciton wavefunction has a substantial spatial extent while the screening from the lattice is weak. Due to strong quantum confinement, excitons in these materials usually have large oscillator strengths and binding energies and are stable even at room temperature.

Graf et al. (2016) demonstrated SC between photons in a FP cavity and excitons in a semiconducting SWCNT-polymer composite, both in reflectivity and photoluminescence, as shown in Fig. 1.20a. In addition to a large VRS exceeding 100 meV, a cooperative enhancement effect with $g \propto \sqrt{N}$ was observed as the SWCNT occupation ratio was systematically adjusted, where N is the number of nanotubes. Graf et al. (2017) further implemented a cavity-integrated light-emitting field effect transistor consisting of a semiconducting SWCNT-polymer composite, which allowed ambipolar charge transport. Under strong current injection, electroluminescence from the LP branch was observed from the low wavevector region of the dispersion, suggesting efficient relaxation. By changing the gate voltage to adjust charge density, the ground state was bleached and overall oscillator strength was reduced. As a result, the VRS decreased, and the system continuously transitioned from strong to weak coupling.

Gao et al. (2018) employed *aligned* SWCNT films also inside a FP cavity and observed a polarization-dependent VRS (Fig. 1.20b), suggesting that the exciton-polaritons inherited anisotropic properties from the SWCNT excitons. Detailed analysis revealed the existence of *exceptional points* in the polariton dispersion surfaces (Fig. 1.20c), where the LP branch and UP branch collapse at the exciton energy. The largest VRS in the thickest device was 329 meV, corresponding to $\eta \approx 0.13$; see Fig. 1.20d. Furthermore, an increase of the film thickness displayed *cooperative enhancement* of g, i.e., VRS was proportional to the square root of the film thickness; see Fig. 1.20e.

1.3.4 Magnon polaritons, spin-magnon coupling, and magnon-magnon coupling

Hybrid quantum systems have seen an increased interest in recent years due to their potential use in quantum communication platforms such as quantum memories, quantum transducers, and quantum information processors [Zhang, Zhu, Zou & Tang (2016), Bittencourt et al. (2019), Zhang et al. (2020)]. In these systems, coupling occurs between two excitations coming from distinctly different constituents, e.g., molecules embedded in optical cavities, exciton-polaritons in a microcavity, and magnons in microwave cavities. In this section, we briefly review some of the recent research efforts on SC and USC phenomena involving magnons.

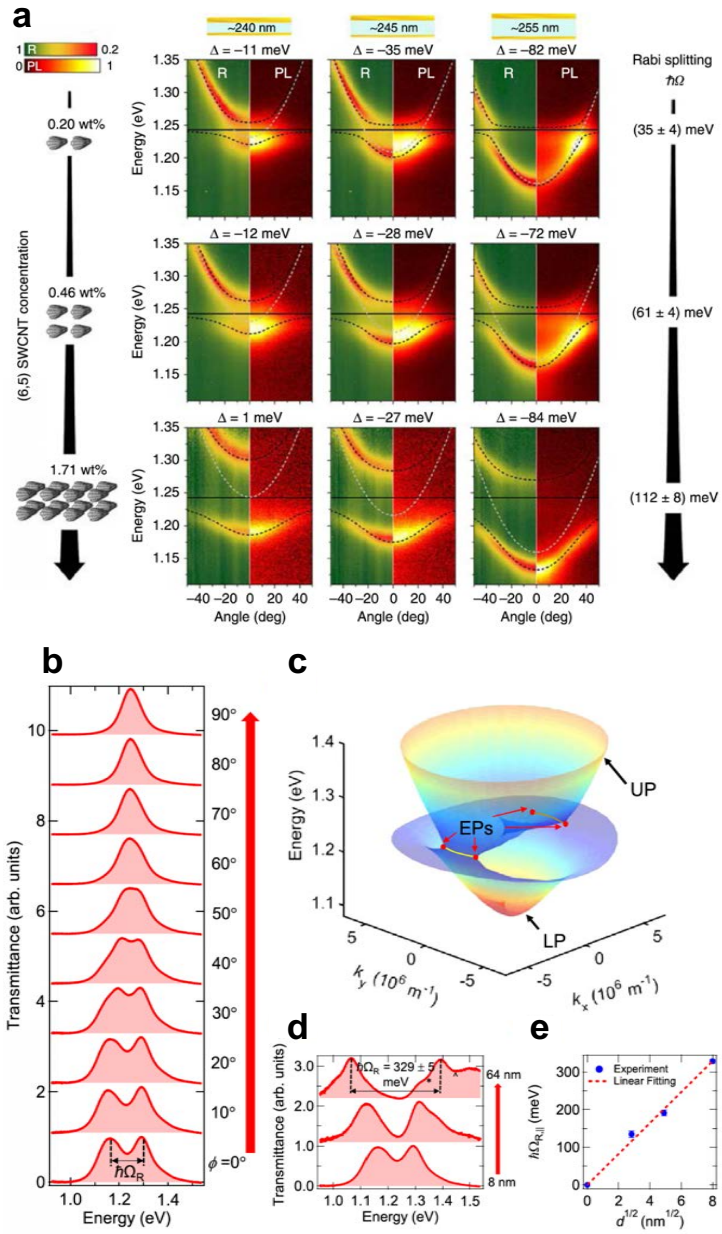

FIGURE 1.20 SC of excitons and photons in semiconducting SWCNTs. (a) Angle-resolved reflectivity and photoluminescence spectra for (6,5) SWCNT microcavity exciton polaritons with increasing nanotube concentration (from top to bottom) and increasing cavity thickness and detuning from (left to right). Adapted from Graf et al. (2016). (b) Transmittance spectra for a cavity containing aligned (6,5) SWCNTs at zero detuning for various polarization angles. (c) The dispersion surfaces of the UP and LP for the device in (b) showing exceptional points (EPs). (d) Transmittance spectra for parallel polarization at zero detuning for devices containing aligned SWCNT films of different thicknesses. The largest VRS is 329 meV for the thickest film. (e) VRS for parallel polarization at zero detuning as a function of the square root of the film thickness, demonstrating collective enhancement. Adapted from Gao et al. (2018).

Cavity optomagnonics, where a set of spin waves (or magnons) collectively couples to the confined electromagnetic field of a cavity [Kusminskiy (2019*a*,*b*), Parvini et al. (2020)], has recently seen some of the first experimental observations of coupling between magnons in the ferrimagnetic insulator YIG to microwave photons both in the SC [Huebl et al. (2013), Tabuchi et al. (2014), Zhang, Zou, Jiang & Tang (2014), Haigh et al. (2015)] and USC [Goryachev et al. (2014)] regimes. Goryachev et al. (2014) observed USC between the magnon resonances of a submillimeter YIG sphere and the bright cavity mode of a double-post 3D microwave reentrant cavity at mK temperatures. Using a novel multipost design [Tobar & Goryachev (2019)], $C \sim 10^5$ was obtained, together with $\eta \sim 0.1$. The cavity transmission as a function of B_{DC} showed a clear anticrossing between the bright cavity mode $f_{\uparrow\downarrow}$ and the magnon mode M_1 (see Fig. 1.21a) and between the dark cavity mode $f_{\uparrow\uparrow}$ and the magnetostatic magnon modes M_2 and M_3. The latter anticrossing showed SC with C reaching 10^3; see Fig. 1.21b. In addition, the authors provided straightforward modifications to the cavity design that could potentially reach $C \sim 10^7$.

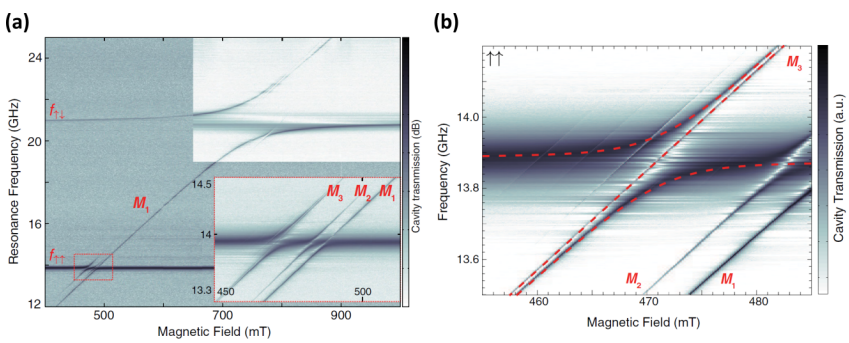

FIGURE 1.21 High-cooperativity cavity QED in the USC regime with magnons at microwave frequencies. (a) Cavity microwave transmission as a function of applied magnetic field, B_{DC}. Anticrossings between the cavity modes $f_{\uparrow\downarrow}$ (bright), $f_{\uparrow\uparrow}$ (dark) and the magnon modes M_1, M_2, and M_3 are observed close to $B_{\mathrm{DC}} = 0.743\,\mathrm{T}$ and $B_{\mathrm{DC}} = 0.471\,\mathrm{T}$, respectively. Inset: zoom-in of the red dashed area shown on the left. (b) Three-mode anticrossing spectra and interacting model fit (red dashed red lines). First-order cancellation of the coupling prohibits the magnon mode M_1 to interact with the dark cavity mode. Adapted from Goryachev et al. (2014).

Recent years have also seen the development of an exciting area of research that focuses on antiferromagnets (AFMs) instead of ferromagnets/ferrimagnets. In AFMs, magnonic excitations typically occur in the THz frequency range and can couple with another degree of freedom coming from the same magnetic system rather than excitations supplied by an external source. For example, a spin-magnon system studied by Li, Bamba, Yuan, Zhang, Zhao, Xiang, Xu, Jin, Ren, Ma, Cao, Turchinovich & Kono (2018) exhibited USC between the electron paramagnetic resonance (EPR) of Er^{3+} spins and the quasi-ferromagnetic ($\mathrm{q_{FM}}$)

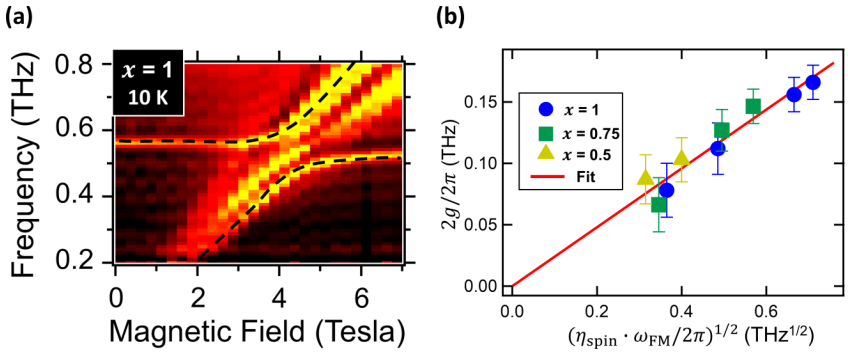

FIGURE 1.22 Dicke cooperativity observed in spin-magnon interactions in the USC regime. (a) Anticrossing behavior at 10 K in the THz frequency range between the Er^{3+} EPR and the Fe^{3+} q_{FM} magnon mode of the rare-earth orthoferrite $Er_xY_{1-x}FeO_3$. An applied magnetic field tunes the EPR with respect to the fixed magnon mode. (b) Cooperative square-root-dependence of the coupling strength g on the number of EPR-contributing spins. Adapted from Li, Bamba, Yuan, Zhang, Zhao, Xiang, Xu, Jin, Ren, Ma, Cao, Turchinovich & Kono (2018).

mode of the Fe^{3+} magnons in the rare-earth orthoferrite, $Er_xY_{1-x}FeO_3$. An applied external DC magnetic field tuned the EPR with respect to the fixed q_{FM} magnon mode frequency, and a clear anticrossing behavior was resolved in the THz range; see Fig. 1.22a. Moreover, a $g \propto \sqrt{N}$ behavior (Dicke cooperativity), where N is the net density of EPR-contributing spins, was obtained; see Fig. 1.22b. The authors estimated a maximum $\eta = 0.18$ in one of the configurations, putting the system in the USC regime. Another example falling in this category is *magnon-magnon coupling* inside a magnetically ordered material [Liensberger et al. (2019), MacNeill et al. (2019), Makihara et al. (2020)]. In these studies, coupling occurred between different magnon modes, and g was tunable by changing the applied magnetic field direction. Makihara et al. (2020) reported USC between the q_{FM} and quasi-antiferromagnetic (q_{AFM}) magnon modes in $YFeO_3$. The authors were able to map the spin model of this system into an *anisotropic* Hopfield Hamiltonian in which the CRTs dominated the co-rotating terms, leading to giant vacuum BS shifts that dominated the shifts due to VRS.

1.4 SUMMARY AND OUTLOOK

In this chapter, we reviewed the theory behind USC and some of the groundbreaking experiments that have taken place since the first theoretical proposal by Ciuti et al. (2005). These pioneering studies have unquestionably shown that the USC regime can be achieved in diverse experimental systems, particularly engineered semiconductor systems. Given the fact that the first experimental

observation of USC was made only eleven years ago at the time of this writing, the fast-paced and continuous progress this field has exhibited in the recent years is truly remarkable. Not only the coupling strengths that can be achieved in experiments have shown an order of magnitude increase during this past decade, but also new and unexplored regimes of light-matter interaction such as the DSC regime have emerged [Yoshihara et al. (2017), Bayer et al. (2017), Mueller et al. (2020)]. The USC regime is now readily accessible using equipment found in most university laboratories around the world.

However, research in this field and our current understanding about it are far from complete. Open questions regarding how to explain some of the experimental observations made in the USC regime remain, and there is much more that can be done on the experimental front to push the boundaries even further to reveal some of the exotic properties predicted for the ground states of systems in the USC regime. In addition, in the same way as applications of light-matter interactions that occur in cavities in the weak and SC regimes advanced the development of solid state lasers, quantum emitters, and precision metrology, the present and future applications of the USC regime are now starting to surface and have found immediate applicability in the long-sought dream of realizing quantum technologies such as quantum computers and quantum simulators. The authors look forward to seeing where this field will be in five, ten, and twenty years from now and what new exciting discoveries will emerge.

ACKNOWLEDGMENTS

The authors thank Takuma Makihara for proofreading the manuscript. J.K. acknowledges support from the U.S. Army Research Office (W911NF-17-1-0259), the U.S. National Science Foundation (NSF MRSEC DMR-1720595), the U.S. Department of Energy (DEFG02-06ER46308), and the Robert A. Welch Foundation (C-1509). M.B. acknowledges support from the Japan Science and Technology Agency (JST) PRESTO program (grant JPMJPR1767).

BIBLIOGRAPHY

Abdurakhimov, L. V., Yamashiro, R., Badrutdinov, A. O. & Konstantinov, D. (2016), 'Strong coupling of the cyclotron motion of surface electrons on liquid helium to a microwave cavity', *Phys. Rev. Lett.* **117**, 056803.

Abragam, A. (1961), *Principles of Nuclear Magnetism*, Oxford University Press, Oxford.

Abram, I. (1987), 'Quantum theory of light propagation: Linear medium', *Phys. Rev. A* **35**, 4661–4672.

Allen, L. & Eberly, J. H. (1975), *Optical Resonance and Two-Level Atoms*, John Wiley & Sons, New York.

Allocca, A. A., Raines, Z. M., Curtis, J. B. & Galitski, V. M. (2019), 'Cavity superconductor-polaritons', *Phys. Rev. B* **99**, 020504.

Amsüss, R., Koller, C., Nöbauer, T., Putz, S., Rotter, S., Sandner, K., Schneider, S., Schramböck, M., Steinhauser, G., Ritsch, H., Schmiedmayer, J. & Majer, J. (2011), 'Cavity QED with magnetically coupled collective spin states', *Phys. Rev. Lett.* **107**, 060502.

Anappara, A. A., Barate, D., Tredicucci, A., Devenson, J., Teissier, R. & Baranov, A. (2007), 'Giant intersubband polariton splitting in InAs/AlSb microcavities', *Solid St. Commun.* **142**, 311–313.

Anappara, A. A., De Liberato, S., Tredicucci, A., Ciuti, C., Biasiol, G., Sorba, L. & Beltram, F. (2009), 'Signatures of the ultrastrong light-matter coupling regime', *Phys. Rev. B* **79**, 201303(R).

Anappara, A. A., Tredicucci, A., Beltram, F., Biasiol, G. & Sorba, L. (2006), 'Tunnel-assisted manipulation of intersubband polaritons in asymmetric coupled quantum wells', *Appl. Phys. Lett.* **89**, 171109.

Anappara, A. A., Tredicucci, A., Biasiol, G. & Sorba, L. (2005), 'Electrical control of polariton coupling in intersubband microcavities', *Appl. Phys. Lett.* **87**, 051105.

Andolina, G., Pellegrino, F., Giovannetti, V., MacDonald, A. & Polini, M. (2019), 'Cavity quantum electrodynamics of strongly correlated electron systems: A no-go theorem for photon condensation', *Phys. Rev. B* **100**, 121109.

Artoni, M. & Birman, J. L. (1989), 'Polariton squeezing: Theory and proposed experiment', *Quant. Opt.* **1**, 91–97.

Artoni, M. & Birman, J. L. (1991), 'Quantum-optical properties of polariton waves', *Phys. Rev. B* **44**, 3736–3756.

Artús, L., Cuscó, R., Ibáñez, J., Blanco, N. & González-Díaz, G. (1999), 'Raman scattering by LO phonon-plasmon coupled modes in *n*-type InP', *Phys. Rev. B* **60**, 5456.

Ashhab, S. & Nori, F. (2010), 'Qubit-oscillator systems in the ultrastrong-coupling regime and their potential for preparing nonclassical states', *Phys. Rev. A* **81**, 042311.

Ashida, Y., Imamoglu, A., Faist, J., Jaksch, D., Cavalleri, A. & Demler, E. (2020), 'Quantum electrodynamic control of matter: Cavity-enhanced ferroelectric phase transition', *arXiv:2003.13695* .

Askenazi, B., Vasanelli, A., Delteil, A., Todorov, Y., Andreani, L. C., Beaudoin, G., Sagnes, I. & Sirtori, C. (2014), 'Ultra-strong light–matter coupling for designer Reststrahlen band', *New J. Phys.* **16**, 043029.

Askenazi, B., Vasanelli, A., Todorov, Y., Sakat, E., Greffet, J.-J., Beaudoin, G., Sagnes, I. & Sirtori, C. (2017), 'Midinfrared ultrastrong light–matter coupling for THz thermal emission', *ACS Photonics* **4**, 2550–2555.

Auer, A. & Burkard, G. (2012), 'Entangled photons from the polariton vacuum in a switchable optical cavity', *Phys. Rev. B* **85**, 235140.

Autore, M., Li, P., Dolado, I., Alfaro-Mozaz, F. J., Esteban, R., Atxabal, A., Casanova, F., Hueso, L. E., Alonso-González, P., Aizpurua, J. et al. (2018), 'Boron nitride nanoresonators for phonon-

enhanced molecular vibrational spectroscopy at the strong coupling limit', *Light: Sci. & Appl.* **7**, 17172–17172.

Ballester, D., Romero, G., García-Ripoll, J. J., Deppe, F. & Solano, E. (2012), 'Quantum simulation of the ultrastrong-coupling dynamics in circuit quantum electrodynamics', *Phys. Rev. X* **2**, 021007.

Bamba, M. & Imoto, N. (2016), 'Maxwell boundary conditions imply non-Lindblad master equation', *Phys. Rev. A* **94**, 033802.

Bamba, M. & Imoto, N. (2017), 'Circuit configurations which may or may not show superradiant phase transitions', *Phys. Rev. A* **96**, 053857.

Bamba, M., Inomata, K. & Nakamura, Y. (2016), 'Superradiant phase transition in a superconducting circuit in thermal equilibrium', *Phys. Rev. Lett.* **117**, 173601.

Bamba, M., Li, X. & Kono, J. (2019), Terahertz strong-field physics without a strong external terahertz field, *in* M. Betz & A. Y. Elezzabi, eds, 'Ultrafast Phenom. Nanophotonics XXIII', SPIE, p. 5.

Bamba, M. & Ogawa, T. (2014), 'Stability of polarizable materials against superradiant phase transition', *Phys. Rev. A* **90**, 063825.

Bamba, M. & Ogawa, T. (2016), 'Laser under ultrastrong light-matter interaction: Qualitative aspects and quantitative influences by level and mode truncations', *Phys. Rev. A* **93**, 033811.

Bao, W., Liu, X., Xue, F., Zheng, F., Tao, R., Wang, S., Xia, Y., Zhao, M., Kim, J., Yang, S. et al. (2019), 'Observation of Rydberg exciton polaritons and their condensate in a perovskite cavity', *Proc. Natl. Acad. Sci. U.S.A.* **116**, 20274–20279.

Bartolo, N. & Ciuti, C. (2018), 'Vacuum-dressed cavity magnetotransport of a two-dimensional electron gas', *Phys. Rev. B* **98**, 205301.

Baumann, K., Guerlin, C., Brennecke, F. & Esslinger, T. (2010), 'Dicke quantum phase transition with a superfluid gas in an optical cavity', *Nature* **464**, 1301–1306.

Bayer, A., Pozimski, M., Schambeck, S., Schuh, D., Huber, R., Bougeard, D. & Lange, C. (2017), 'Terahertz light–matter interaction beyond unity coupling strength', *Nano Lett.* **17**, 6340–6344.

Bialynicki-Birula, I. & Rzażewski, K. (1979), 'No-go theorem concerning the superradiant phase transition in atomic systems', *Phys. Rev. A* **19**, 301–303.

Bittencourt, V. A., Feulner, V. & Kusminskiy, S. V. (2019), 'Magnon heralding in cavity opto-magnonics', *Phys. Rev. A* **100**, 013810.

Bloch, F. & Siegert, A. (1940), 'Magnetic resonance for nonrotating fields', *Phys. Rev.* **57**, 522–527.

Bloch, J., Freixanet, T., Marzin, J. Y., Thierry-Mieg, V. & Planel, R. (1998), 'Giant Rabi splitting in a microcavity containing distributed quantum wells', *Appl. Phys. Lett.* **73**, 1694–1696.

Bonifacio, R. & Lugiato, L. A. (1982), Theory of optical bistability, *in* R. Bonifacio, ed., 'Dissipative Systems in Quantum Optics', Topics in Current Physics, Springer-Verlag, Berlin, chapter 4, pp. 61–92.

Brar, V. W., Jang, M. S., Sherrott, M., Kim, S., Lopez, J. J., Kim, L. B., Choi, M. & Atwater, H. (2014), 'Hybrid surface-phonon-plasmon polariton modes in graphene/monolayer h-BN heterostructures', *Nano Lett.* **14**, 3876–3880.

Brey, L., Johnson, N. F. & Halperin, B. I. (1989), 'Optical and magneto-optical absorption in parabolic quantum wells', *Phys. Rev. B* **40**, 10647–10649.

Caldwell, J. D., Kretinin, A. V., Chen, Y., Giannini, V., Fogler, M. M., Francescato, Y., Ellis, C. T., Tischler, J. G., Woods, C. R., Giles, A. J. et al. (2014), 'Sub-diffractional volume-confined polaritons in the natural hyperbolic material hexagonal boron nitride', *Nat. Commun.* **5**, 1–9.

Caldwell, J. D., Lindsay, L., Giannini, V., Vurgaftman, I., Reinecke, T. L., Maier, S. A. & Glembocki, O. J. (2015), 'Low-loss, infrared and terahertz nanophotonics using surface phonon polaritons', *Nanophotonics* **4**, 44–68.

Caldwell, J. D., Vurgaftman, I., Tischler, J. G., Glembocki, O. J., Owrutsky, J. C. & Reinecke,

T. L. (2016), 'Atomic-scale photonic hybrids for mid-infrared and terahertz nanophotonics', *Nat. Nanotechnol.* **11**, 9–15.

Carusotto, I., De Liberato, S., Gerace, D. & Ciuti, C. (2012), 'Back-reaction effects of quantum vacuum in cavity quantum electrodynamics', *Phys. Rev. A* **85**, 23805.

Casanova, J., Romero, G., Lizuain, I., García-Ripoll, J. J. & Solano, E. (2010), 'Deep strong coupling regime of the Jaynes-Cummings model', *Phys. Rev. Lett.* **105**, 263603.

Chafai, M., Jaouhari, A., Torres, A., Antón, R., Martın, E., Jiménez, J. & Mitchel, W. (2001), 'Raman scattering from LO phonon-plasmon coupled modes and Hall-effect in n-type silicon carbide 4H–SiC', *J. Appl. Phys.* **90**, 5211–5215.

Chandrasekhar, H. & Ramdas, A. (1980), 'Nonparabolicity of the conduction band and the coupled plasmon-phonon modes in n-GaAs', *Phys. Rev. B* **21**, 1511.

Chen, J., Badioli, M., Alonso-González, P., Thongrattanasiri, S., Huth, F., Osmond, J., Spasenović, M., Centeno, A., Pesquera, A., Godignon, P. et al. (2012), 'Optical nano-imaging of gate-tunable graphene plasmons', *Nature* **487**, 77–81.

Chen, J.-R., Lu, T.-C., Wu, Y.-C., Lin, S.-C., Hsieh, W.-F., Wang, S.-C. & Deng, H. (2011), 'Characteristics of exciton-polaritons in ZnO-based hybrid microcavities', *Opt. Exp.* **19**, 4101–4112.

Chen, T., Liu, P., Liu, J. & Hong, Z. (2014), 'A terahertz photonic crystal cavity with high Q-factors', *Appl. Phys. B* **115**, 105–109.

Chen, Y., Francescato, Y., Caldwell, J. D., Giannini, V., Maß, T. W., Glembocki, O. J., Bezares, F. J., Taubner, T., Kasica, R., Hong, M. et al. (2014), 'Spectral tuning of localized surface phonon polariton resonators for low-loss mid-IR applications', *ACS Photon.* **1**, 718–724.

Chen, Y.-J., Cain, J. D., Stanev, T. K., Dravid, V. P. & Stern, N. P. (2017), 'Valley-polarized exciton–polaritons in a monolayer semiconductor', *Nat. Photonics* **11**, 431–435.

Chirolli, L., Polini, M., Giovannetti, V. & MacDonald, A. H. (2012), 'Drude weight, cyclotron resonance, and the Dicke model of graphene cavity QED', *Phys. Rev. Lett.* **109**, 267404.

Choi, K.-K. (1997), *The Physics of Quantum Well Infrared Photodetectors*, Vol. 7, World Scientific, Singapore.

Christmann, G., Butté, R., Feltin, E., Carlin, J.-F. & Grandjean, N. (2008), 'Room temperature polariton lasing in a GaN/AlGaN multiple quantum well microcavity', *Appl. Phys. Lett.* **93**, 051102.

Cirio, M., De Liberato, S., Lambert, N. & Nori, F. (2016), 'Ground state electroluminescence', *Phys. Rev. Lett.* **116**, 113601.

Cirio, M., Debnath, K., Lambert, N. & Nori, F. (2017), 'Amplified optomechanical transduction of virtual radiation pressure', *Phys. Rev. Lett.* **119**, 053601.

Cirio, M., Shammah, N., Lambert, N., De Liberato, S. & Nori, F. (2019), 'Multielectron ground state electroluminescence', *Phys. Rev. Lett.* **122**, 190403.

Ciuti, C., Bastard, G. & Carusotto, I. (2005), 'Quantum vacuum properties of the intersubband cavity polariton field', *Phys. Rev. B* **72**, 115303.

Ciuti, C. & Carusotto, I. (2006), 'Input-output theory of cavities in the ultrastrong coupling regime: The case of time-independent cavity parameters', *Phys. Rev. A* **74**, 033811.

Ciuti, C. & Nataf, P. (2012), 'Comment on "superradiant phase transitions and the standard description of circuit QED"', *Phys. Rev. Lett.* **109**, 179301.

Cohen-Tannoudji, C., Dupont-Roc, J. & Fabre, C. (1973), 'A quantum calculation of the higher order terms in the Bloch-Siegert shift', *J. Phys. B* **6**, L214–L217.

Cohen-Tannoudji, C., Dupont-Roc, J. & Grynberg, G. (1989), *Photons and Atoms: Introduction to Quantum Electrodynamics*, John Wiley & Sons, Inc., New York.

Combescot, M., Betbedermatibet, O. & Dubin, F. (2008), 'The many-body physics of composite bosons', *Phys. Rep.* **463**, 215–320.

Curtis, J. B., Raines, Z. M., Allocca, A. A., Hafezi, M. & Galitski, V. M. (2019), 'Cavity quantum Eliashberg enhancement of superconductivity', *Phys. Rev. Lett.* **122**, 167002.

Dai, S., Ma, Q., Liu, M., Andersen, T., Fei, Z., Goldflam, M., Wagner, M., Watanabe, K., Taniguchi, T., Thiemens, M. et al. (2015), 'Graphene on hexagonal boron nitride as a tunable hyperbolic metamaterial', *Nat. Nanotechnol.* **10**, 682–686.

De Bernardis, D., Pilar, P., Jaako, T., De Liberato, S. & Rabl, P. (2018), 'Breakdown of gauge invariance in ultrastrong-coupling cavity QED', *Phys. Rev. A* **98**, 053819.

De Liberato, S. (2014), 'Light-matter decoupling in the deep strong coupling regime: The breakdown of the Purcell effect', *Phys. Rev. Lett.* **112**, 016401.

De Liberato, S., Ciuti, C. & Carusotto, I. (2007), 'Quantum vacuum radiation spectra from a semiconductor microcavity with a time-modulated vacuum Rabi frequency', *Phys. Rev. Lett.* **98**, 103602.

De Liberato, S., Gerace, D., Carusotto, I. & Ciuti, C. (2009), 'Extracavity quantum vacuum radiation from a single qubit', *Phys. Rev. A* **80**, 53810.

De Zela, F., Solano, E. & Gago, A. (1997), 'Micromaser without the rotating-wave approximation: The Bloch-Siegert shift and related effects', *Opt. Commun.* **142**, 106–118.

Delteil, A., Vasanelli, A., Todorov, Y., Feuillet Palma, C., Renaudat St-Jean, M., Beaudoin, G., Sagnes, I. & Sirtori, C. (2012), 'Charge-induced coherence between intersubband plasmons in a quantum structure', *Phys. Rev. Lett.* **109**, 246808.

Deng, H., Haug, H. & Yamamoto, Y. (2010), 'Exciton-polariton Bose-Einstein condensation', *Rev. Mod. Phys.* **82**, 1489–1537.

Deng, H., Weihs, G., Santori, C., Bloch, J. & Yamamoto, Y. (2002), 'Condensation of semiconductor microcavity exciton polaritons', *Science* **298**(5591), 199–202.

Di Stefano, O., Settineri, A., Macrì, V., Garziano, L., Stassi, R., Savasta, S. & Nori, F. (2019), 'Resolution of gauge ambiguities in ultrastrong-coupling cavity QED', *Nat. Phys.* **15**, 803–808.

Dicke, R. H. (1954), 'Coherence in spontaneous radiation processes', *Phys. Rev.* **93**, 99–110.

Dietze, D., Andrews, A. M., Klang, P., Strasser, G., Unterrainer, K. & Darmo, J. (2013), 'Ultrastrong coupling of intersubband plasmons and terahertz metamaterials', *Appl. Phys. Lett.* **103**, 201106.

Dimer, F., Estienne, B., Parkins, A. S. & Carmichael, H. J. (2007), 'Proposed realization of the Dicke-model quantum phase transition in an optical cavity QED system', *Phys. Rev. A* **75**, 013804.

Dini, D., Köhler, R., Tredicucci, A., Biasiol, G. & Sorba, L. (2003), 'Microcavity polariton splitting of intersubband transitions', *Phys. Rev. Lett.* **90**, 116401.

Dodonov, A. V., Celeri, L. C., Pascoal, F., Lukin, M. D. & Yelin, S. F. (2008), 'Photon generation from vacuum in non-stationary circuit QED', *arXiv:0806:4035* .

Drozdov, A., Kong, P., Minkov, V., Besedin, S., Kuzovnikov, M., Mozaffari, S., Balicas, L., Balakirev, F., Graf, D., Prakapenka, V. et al. (2019), 'Superconductivity at 250 k in lanthanum hydride under high pressures', *Nature* **569**, 528–531.

Dufferwiel, S., Lyons, T., Solnyshkov, D., Trichet, A., Withers, F., Schwarz, S., Malpuech, G., Smith, J., Novoselov, K., Skolnick, M. et al. (2017), 'Valley-addressable polaritons in atomically thin semiconductors', *Nat. Photon.* **11**, 497–501.

Dufferwiel, S., Schwarz, S., Withers, F., Trichet, A., Li, F., Sich, M., Del Pozo-Zamudio, O., Clark, C., Nalitov, A., Solnyshkov, D. et al. (2015), 'Exciton–polaritons in van der Waals heterostructures embedded in tunable microcavities', *Nat. Commun.* **6**, 1–7.

Dupont, E., Gupta, J. A. & Liu, H. C. (2007), 'Giant vacuum-field Rabi splitting of intersubband transitions in multiple quantum wells', *Phys. Rev. B* **75**, 205325.

Dupont, E., Liu, H. C., SpringThorpe, A. J., Lai, W. & Extavour, M. (2003), 'Vacuum-field Rabi splitting in quantum-well infrared photodetectors', *Phys. Rev. B* **68**, 245320.

Eliashberg, G. M. (1970), 'Film superconductivity stimulated by a high-frequency field', *JETP Lett.*

11, 114–116.

Emary, C. & Brandes, T. (2003*a*), 'Chaos and the quantum phase transition in the Dicke model', *Phys. Rev. E* **67**, 066203.

Emary, C. & Brandes, T. (2003*b*), 'Quantum chaos triggered by precursors of a quantum phase transition: The dicke model', *Phys. Rev. Lett.* **90**, 044101.

Faist, J., Capasso, F., Sivco, D. L., Sirtori, C., Hutchinson, A. L. & Cho, A. Y. (1994), 'Quantum cascade laser', *Science* **264**, 553–556.

Fei, Z., Rodin, A. S., Andreev, G. O., Bao, W., McLeod, A. S., Wagner, M., Zhang, L. M., Zhao, Z., Thiemens, M., Dominguez, G., Fogler, M. M., Castro Neto, A. H., Lau, C. N., Keilmann, F. & Basov, D. N. (2012), 'Gate-tuning of graphene plasmons revealed by infrared nano-imaging', *Nature* **487**, 82–85.

Felicetti, S., Douce, T., Romero, G., Milman, P. & Solano, E. (2015), 'Parity-dependent state engineering and tomography in the ultrastrong coupling regime', *Sci. Rep.* **5**, 11818.

Ferrari, L., Wu, C., Lepage, D., Zhang, X. & Liu, Z. (2015), 'Hyperbolic metamaterials and their applications', *Prog. Quantum Electron.* **40**, 1–40.

Ferraro, D., Andolina, G. M., Campisi, M., Pellegrini, V. & Polini, M. (2019), 'Quantum supercapacitors', *Phys. Rev. B* **100**, 075433.

Ferraro, D., Campisi, M., Andolina, G. M., Pellegrini, V. & Polini, M. (2018), 'High-power collective charging of a solid-state quantum battery', *Phys. Rev. Lett.* **120**, 117702.

Ferraro, D., Campisi, M., Andolina, G. M., Pellegrini, V. & Polini, M. (2020), 'Quantum resources for energy storage', *EPJ Web Conf.* **230**, 00003.

Flower, G., Bourhill, J., Goryachev, M. & Tobar, M. E. (2019), 'Broadening frequency range of a ferromagnetic axion haloscope with strongly coupled cavity-magnon polaritons', *Phys. Dark Universe* **25**, 100306.

Flower, G., Goryachev, M., Bourhill, J. & Tobar, M. E. (2019), 'Experimental implementations of cavity-magnon systems: from ultrastrong coupling to applications in precision measurement', *New J. Phys.* **21**, 095004.

Forn-Díaz, P., Lamata, L., Rico, E., Kono, J. & Solano, E. (2019), 'Ultrastrong coupling regimes of light-matter interaction', *Rev. Mod. Phys.* **91**, 025005.

Fulling, S. A. & Davies, P. C. W. (1976), 'Radiation from a moving mirror in two dimensional space-time: Conformal anomaly', *Proc. Roy. Soc. London A* **348**, 393–414.

Gambino, S., Mazzeo, M., Genco, A., Di Stefano, O., Savasta, S., Patanè, S., Ballarini, D., Mangione, F., Lerario, G., Sanvitto, D. et al. (2014), 'Exploring light–matter interaction phenomena under ultrastrong coupling regime', *ACS Photonics* **1**, 1042–1048.

Gao, H., Schlawin, F., Buzzi, M., Cavalleri, A. & Jaksch, D. (2020), 'Photoinduced electron pairing in a driven cavity', *Phys. Rev. Lett.* **125**, 053602.

Gao, W., Li, X., Bamba, M. & Kono, J. (2018), 'Continuous transition between weak and ultrastrong coupling through exceptional points in carbon nanotube microcavity exciton–polaritons', *Nat. Photon.* **12**, 362–367.

Gao, W., Shi, G., Jin, Z., Zhang, Q., Ajayan, P. M., Kono, J. & Xu, Q. (2013), 'Excitation and active control of propagating surface plasmon polaritons in graphene', *Nano Lett.* **13**, 3698–3702.

Gao, W., Shu, J., Qiu, C. & Xu, Q. (2012), 'Excitation of plasmonic waves in graphene by guided-mode resonances', *ACS Nano* **6**, 7806–7813.

Gao, W., Shu, J., Reichel, K., Nickel, D., He, X., Shi, G., Vajtai, R., Ajayan, P. M., Kono, J., Mittleman, D. M. & Xu, Q. (2014), 'High-contrast terahertz wave modulation by gated graphene enhanced by extraordinary transmission through ring apertures', *Nano Lett.* **14**, 1242–1248.

Garziano, L., Ridolfo, A., Stassi, R., Di Stefano, O. & Savasta, S. (2013), 'Switching on and off of ultrastrong light-matter interaction: Photon statistics of quantum vacuum radiation', *Phys. Rev. A*

88, 63829.

Garziano, L., Settineri, A., Di Stefano, O., Savasta, S. & Nori, F. (2020), 'Gauge invariance of the Dicke and Hopfield models', *arXiv:2002.04241* .

Garziano, L., Stassi, R., Ridolfo, A., Di Stefano, O. & Savasta, S. (2014), 'Vacuum-induced symmetry breaking in a superconducting quantum circuit', *Phys. Rev. A* **90**, 43817.

Gaur, N. (1976), 'Longitudinal optical phonon-plasmon coupling in InSb and InAs', *Physica B+C* **82**, 262–270.

Gawędzki, K. & Rzążewski, K. (1981), 'No-go theorem for the superradiant phase transition without dipole approximation', *Phys. Rev. A* **23**, 2134–2136.

Geiser, M., Castellano, F., Scalari, G., Beck, M., Nevou, L. & Faist, J. (2012), 'Ultrastrong coupling regime and plasmon polaritons in parabolic semiconductor quantum wells', *Phys. Rev. Lett.* **108**, 106402.

Geiser, M., Walther, C., Scalari, G., Beck, M., Fischer, M., Nevou, L. & Faist, J. (2010), 'Strong light-matter coupling at terahertz frequencies at room temperature in electronic LC resonators', *Appl. Phys. Lett.* **97**, 191107.

Gibbs, H. M., Khitrova, G. & Koch, S. W. (2011), 'Exciton-polariton light-semiconductor coupling effects', *Nat. Photon.* **5**, 273–273.

Glauber, R. J. & Lewenstein, M. (1991), 'Quantum optics of dielectric media', *Phys. Rev. A* **43**, 467–491.

Goryachev, M., Farr, W. G., Creedon, D. L., Fan, Y., Kostylev, M. & Tobar, M. E. (2014), 'High-cooperativity cavity QED with magnons at microwave frequencies', *Phys. Rev. Applied* **2**, 054002.

Graf, A., Held, M., Zakharko, Y., Tropf, L., Gather, M. C. & Zaumseil, J. (2017), 'Electrical pumping and tuning of exciton-polaritons in carbon nanotube microcavities', *Nat. Mater.* **16**, 911–917.

Graf, A., Tropf, L., Zakharko, Y., Zaumseil, J. & Gather, M. C. (2016), 'Near-infrared exciton-polaritons in strongly coupled single-walled carbon nanotube microcavities', *Nat. Commun.* **7**, 13078.

Grießer, T., Vukics, A. & Domokos, P. (2016), 'Depolarization shift of the superradiant phase transition', *Phys. Rev. A* **94**, 033815.

Grigorenko, A., Polini, M. & Novoselov, K. (2012), 'Graphene plasmonics', *Nat. Photon.* **6**, 749–758.

Guillet, T., Mexis, M., Levrat, J., Rossbach, G., Brimont, C., Bretagnon, T., Gil, B., Butté, R., Grandjean, N., Orosz, L., Réveret, F., Leymarie, J., Zúñiga-Pérez, J., Leroux, M., Semond, F. & Bouchoule, S. (2011), 'Polariton lasing in a hybrid bulk ZnO microcavity', *Appl. Phys. Lett.* **99**, 161104.

Günter, G., Anappara, A. A., Hees, J., Sell, A., Biasiol, G., Sorba, L., De Liberato, S., Ciuti, C., Tredicucci, A., Leitenstorfer, A. & Huber, R. (2009), 'Sub-cycle switch-on of ultrastrong light–matter interaction', *Nature* **458**, 178–181.

Hagenmüller, D. (2016), 'All-optical dynamical Casimir effect in a three-dimensional terahertz photonic band gap', *Phys. Rev. B* **93**, 235309.

Hagenmüller, D. & Ciuti, C. (2012), 'Cavity QED of the graphene cyclotron transition', *Phys. Rev. Lett.* **109**, 267403.

Haigh, J., Lambert, N., Doherty, A. & Ferguson, A. (2015), 'Dispersive readout of ferromagnetic resonance for strongly coupled magnons and microwave photons', *Phys. Rev. B* **91**, 104410.

Harima, H., Nakashima, S.-i. & Uemura, T. (1995), 'Raman scattering from anisotropic LO-phonon–plasmon–coupled mode in *n*-type 4H–and 6H–SiC', *J. Appl. Phys.* **78**, 1996–2005.

Hasselbeck, M., Stalnaker, D., Schlie, L., Rotter, T., Stintz, A. & Sheik-Bahae, M. (2002), 'Emission of terahertz radiation from coupled plasmon-phonon modes in InAs', *Phys. Rev. B* **65**, 233203.

Hawking, S. W. (1974), 'Black hole explosions?', *Nature (London)* **248**, 30–31.

Hawking, S. W. (1975), 'Particle creation by black holes', *Commun. Math. Phys.* **43**, 199–220.

Helm, M. (2000), The basic physics of intersubband transitions, *in* H. C. Liu & F. Capasso, eds, 'Intersubband Transitions in Quantum Wells: Physics and Device Applications I', Vol. 62 of *Semiconductors and Semimetals*, Academic Press, San Diego, pp. 1–99.

Hepp, K. & Lieb, E. H. (1973), 'On the superradiant phase transition for molecules in a quantized radiation field: the Dicke maser model', *Ann. Phys.* **76**, 360–404.

Hilton, D. J., Arikawa, T. & Kono, J. (2012), Cyclotron resonance, *in* E. N. Kaufmann, ed., 'Characterization of Materials', 2nd edn, John Wiley & Sons, Inc., New York, pp. 1–15.

Hoffman, A. J., Alekseyev, L., Howard, S. S., Franz, K. J., Wasserman, D., Podolskiy, V. A., Narimanov, E. E., Sivco, D. L. & Gmachl, C. (2007), 'Negative refraction in semiconductor metamaterials', *Nat. Mater.* **6**, 946–950.

Hopfield, J. J. (1958), 'Theory of the contribution of excitons to the complex dielectric constant of crystals', *Phys. Rev.* **112**, 1555–1567.

Huang, J. F. & Law, C. K. (2014), 'Photon emission via vacuum-dressed intermediate states under ultrastrong coupling', *Phys. Rev. A* **89**, 033827.

Huebl, H., Zollitsch, C. W., Lotze, J., Hocke, F., Greifenstein, M., Marx, A., Gross, R. & Goennenwein, S. T. (2013), 'High cooperativity in coupled microwave resonator ferrimagnetic insulator hybrids', *Phys. Rev. Lett.* **111**, 127003.

Hwang, M.-J., Puebla, R. & Plenio, M. B. (2015), 'Quantum phase transition and universal dynamics in the Rabi model', *Phys. Rev. Lett.* **115**, 180404.

Jaako, T., Xiang, Z.-L., Garcia-Ripoll, J. J. & Rabl, P. (2016), 'Ultrastrong-coupling phenomena beyond the Dicke model', *Phys. Rev. A* **94**, 033850.

Jablan, M., Buljan, H. & Soljačić, M. (2009), 'Plasmonics in graphene at infrared frequencies', *Phys. Rev. B* **80**, 245435.

Jeannin, M., Mariotti Nesurini, G., Suffit, S., Gacemi, D., Vasanelli, A., Li, L., Davies, A. G., Linfield, E., Sirtori, C. & Todorov, Y. (2019), 'Ultrastrong light–matter coupling in deeply subwavelength THz LC resonators', *ACS Photonics* **6**, 1207–1215.

Jia, Y., Zhao, H., Guo, Q., Wang, X., Wang, H. & Xia, F. (2015), 'Tunable plasmon–phonon polaritons in layered graphene–hexagonal boron nitride heterostructures', *ACS Photon.* **2**, 907–912.

Jouy, P., Vasanelli, A., Todorov, Y., Delteil, A., Biasiol, G., Sorba, L. & Sirtori, C. (2011), 'Transition from strong to ultrastrong coupling regime in mid-infrared metal-dielectric-metal cavities', *Appl. Phys. Lett.* **98**, 231114.

Ju, L., Geng, B., Horng, J., Girit, C., Martin, M., Hao, Z., Bechtel, H. A., Liang, X., Zettl, A., Shen, Y. R. & Wang, F. (2011), 'Graphene plasmonics for tunable terahertz metamaterials', *Nat. Nanotechnol.* **6**, 630–634.

Juraschek, D. M., Neuman, T., Flick, J. & Narang, P. (2019), 'Cavity control of nonlinear phononics', *arXiv:1912.00122* .

Kaiser, S. (2017), 'Light-induced superconductivity in high-Tc cuprates', *Phys. Script.* **92**, 103001.

Kaluzny, Y., Goy, P., Gross, M., Raimond, J. M. & Haroche, S. (1983), 'Observation of self-induced Rabi oscillations in two-level atoms excited inside a resonant cavity: The ringing regime of superradiance', *Phys. Rev. Lett.* **51**, 1175–1178.

Kardar, M. & Golestanian, R. (1999), 'The "friction" of vacuum, and other fluctuation-induced forces', *Rev. Mod. Phys.* **71**, 1233–1245.

Keeling, J. (2007), 'Coulomb interactions, gauge invariance, and phase transitions of the Dicke model', *J. Phys. Condens. Matter* **19**, 295213.

Keller, J., Scalari, G., Appugliese, F., Mavrona, E., Rajabali, S., Süess, M. J., Beck, M. & Faist, J. (2018), 'High Tc superconducting THz metamaterial for ultrastrong coupling in a magnetic field', *ACS Photonics* **5**, 3977–3983.

Keller, J., Scalari, G., Appugliese, F., Rajabali, S., Beck, M., Haase, J., Lehner, C. A., Wegscheider, W., Failla, M., Myronov, M., Leadley, D. R., Lloyd-Hughes, J., Nataf, P. & Faist, J. (2020), 'Landau polaritons in highly nonparabolic two-dimensional gases in the ultrastrong coupling regime', *Phys. Rev. B* **101**, 075301.

Keller, J., Scalari, G., Cibella, S., Maissen, C., Appugliese, F., Giovine, E., Leoni, R., Beck, M. & Faist, J. (2017), 'Few-electron ultrastrong light-matter coupling at 300 GHz with nanogap hybrid LC microcavities', *Nano Lett.* **17**, 7410–7415.

Kéna-Cohen, S. & Forrest, S. R. (2010), 'Room-temperature polariton lasing in an organic single-crystal microcavity', *Nat. Photon.* **4**, 371–375.

Khitrova, G., Gibbs, H. M., Jahnke, F., Kira, M. & Koch, S. W. (1999), 'Nonlinear optics of normal-mode-coupling semiconductor microcavities', *Rev. Mod. Phys.* **71**, 1591–1639.

Khurgin, J. B. (2015), 'How to deal with the loss in plasmonics and metamaterials', *Nat. Nanotechnol.* **10**, 2–6.

Kiffner, M., Coulthard, J. R., Schlawin, F., Ardavan, A. & Jaksch, D. (2019), 'Manipulating quantum materials with quantum light', *Phys. Rev. B* **99**, 085116.

Kim, O. & Spitzer, W. (1979), 'Study of plasmon–LO-phonon coupling in Te-doped $Ga_{1-x}Al_xAs$', *Phys. Rev. B* **20**, 3258.

Klein, M. V., Ganguly, B. & Colwell, P. J. (1972), 'Theoretical and experimental study of Raman scattering from coupled LO-phonon-plasmon modes in silicon carbide', *Phys. Rev. B* **6**, 2380.

Knight, J. M., Aharonov, Y. & Hsieh, G. T. C. (1978), 'Are super-radiant phase transitions possible?', *Phys. Rev. A* **17**, 1454–1462.

Kockum, A. F., Miranowicz, A., De Liberato, S., Savasta, S. & Nori, F. (2019), 'Ultrastrong coupling between light and matter', *Nat. Rev. Phys.* **1**, 19–40.

Kohn, W. (1961), 'Cyclotron resonance and de Haas-van Alphen oscillations of an interacting electron gas', *Phys. Rev.* **123**, 1242.

Kono, J. (2001), Cyclotron resonance, *in* E. N. Kaufmann, R. Abbaschian, A. Bocarsly, C.-L. Chien, D. Dollimore, B. Doyle, A. Goldman, R. Gronsky, S. Pearton & J. Sanchez, eds, 'Methods in Materials Research', John Wiley & Sons, New York, chapter 9b.2.

Koppens, F. H., Chang, D. E. & Garcia de Abajo, F. J. (2011), 'Graphene plasmonics: a platform for strong light–matter interactions', *Nano Lett.* **11**, 3370–3377.

Kozawa, T., Kachi, T., Kano, H., Taga, Y., Hashimoto, M., Koide, N. & Manabe, K. (1994), 'Raman scattering from LO phonon-plasmon coupled modes in gallium nitride', *J. Appl. Phys.* **75**, 1098–1101.

Kukharskii, A. (1973), 'Plasmon-phonon coupling in GaAs', *Solid St. Commun.* **13**, 1761–1765.

Kusminskiy, S. V. (2019*a*), 'Cavity optomagnonics', *arXiv:1911.11104* .

Kusminskiy, S. V. (2019*b*), *Quantum Magnetism, Spin Waves, and Optical Cavities*, Springer, Berlin.

Kyaw, T. H., Felicetti, S., Romero, G., Solano, E. & Kwek, L. C. (2015), 'Scalable quantum memory in the ultrastrong coupling regime', *Sci. Rep.* **5**, 8621.

Kyaw, T. H., Herrera-Martí, D. A., Solano, E., Romero, G. & Kwek, L.-C. (2015), 'Creation of quantum error correcting codes in the ultrastrong coupling regime', *Phys. Rev. B* **91**, 064503.

Lamata, L. (2017), 'Digital-analog quantum simulation of generalized Dicke models with superconducting circuits', *Sci. Rep.* **7**, 43768.

Larson, J. & Irish, E. K. (2017), 'Some remarks on 'superradiant' phase transitions in light-matter systems', *J. Phys. A: Math. Theor.* **50**, 174002.

Latini, S., Ronca, E., De Giovannini, U., Hübener, H. & Rubio, A. (2019), 'Cavity control of excitons in two-dimensional materials', *Nano Lett.* **19**, 3473–3479.

Laurent, T., Manceau, J.-M., Monroy, E., Lim, C., Rennesson, S., Semond, F., Julien, F. & Colombelli, R. (2017), 'Short-wave infrared ($\lambda = 3\ \mu$m) intersubband polaritons in the GaN/AlN

system', *Appl. Phys. Lett.* **110**, 131102.

Law, S., Adams, D., Taylor, A. & Wasserman, D. (2012), 'Mid-infrared designer metals', *Opt. Express* **20**, 12155–12165.

Lax, B. & Mavroides, J. G. (1960), Cyclotron resonance, *in* F. Seitz & D. Turnbull, eds, 'Solid State Physics', Vol. 11, Academic Press, New York, pp. 261–400.

Lee, B., Liu, W., Naylor, C. H., Park, J., Malek, S. C., Berger, J. S., Johnson, A. T. C. & Agarwal, R. (2017), 'Electrical tuning of exciton–plasmon polariton coupling in monolayer MoS_2 integrated with plasmonic nanoantenna lattice', *Nano Lett.* **17**, 4541–4547.

Li, X., Bamba, M., Yuan, N., Zhang, Q., Zhao, Y., Xiang, M., Xu, K., Jin, Z., Ren, W., Ma, G., Cao, S., Turchinovich, D. & Kono, J. (2018), 'Observation of Dicke cooperativity in magnetic interactions', *Science* **361**(6404), 794–797.

Li, X., Bamba, M., Zhang, Q., Fallahi, S., Gardner, G. C., Gao, W., Lou, M., Yoshioka, K., Manfra, M. J. & Kono, J. (2018), 'Vacuum Bloch–Siegert shift in Landau polaritons with ultra-high cooperativity', *Nat. Photon.* **12**, 324–329.

Lidzey, D. G., Bradley, D. D. C., Skolnick, M. S., Virgili, T., Walker, S. & Whittaker, D. M. (1998), 'Strong exciton–photon coupling in an organic semiconductor microcavity', *Nature* **395**, 53–55.

Liensberger, L., Kamra, A., Maier-Flaig, H., Geprägs, S., Erb, A., Goennenwein, S. T., Gross, R., Belzig, W., Huebl, H. & Weiler, M. (2019), 'Exchange-enhanced ultrastrong magnon-magnon coupling in a compensated ferrimagnet', *Phys. Rev. Lett.* **123**, 117204.

Liu, A. (1997), 'Rabi splitting of the optical intersubband absorption line of multiple quantum wells inside a Fabry-Pérot microcavity', *Phys. Rev. B* **55**, 7101–7109.

Liu, W., Lee, B., Naylor, C. H., Ee, H.-S., Park, J., Johnson, A. T. C. & Agarwal, R. (2016), 'Strong exciton–plasmon coupling in MoS_2 coupled with plasmonic lattice', *Nano Lett.* **16**, 1262–1269.

Liu, X., Galfsky, T., Sun, Z., Xia, F., Lin, E.-c., Lee, Y.-H., Kéna-Cohen, S. & Menon, V. M. (2015), 'Strong light–matter coupling in two-dimensional atomic crystals', *Nat. Photon.* **9**, 30–34.

Lolli, J., Baksic, A., Nagy, D., Manucharyan, V. E. & Ciuti, C. (2015), 'Ancillary qubit spectroscopy of vacua in cavity and circuit quantum electrodynamics', *Phys. Rev. Lett.* **114**, 183601.

Luttinger, J. M. & Kohn, W. (1955), 'Motion of electrons and holes in perturbed periodic fields', *Phys. Rev.* **97**, 869–883.

MacNeill, D., Hou, J. T., Klein, D. R., Zhang, P., Jarillo-Herrero, P. & Liu, L. (2019), 'Gigahertz frequency antiferromagnetic resonance and strong magnon-magnon coupling in the layered crystal $crcl_3$', *Phys. Rev. Lett.* **123**, 047204.

Maissen, C., Scalari, G., Beck, M. & Faist, J. (2017), 'Asymmetry in polariton dispersion as function of light and matter frequencies in the ultrastrong coupling regime', *New J. Phys.* **19**, 043022.

Maissen, C., Scalari, G., Valmorra, F., Beck, M., Faist, J., Cibella, S., Leoni, R., Reichl, C., Charpentier, C. & Wegscheider, W. (2014), 'Ultrastrong coupling in the near field of complementary split-ring resonators', *Phys. Rev. B* **90**, 205309.

Makihara, T., Hayashida, K., Noe II, G. T., Li, X., Marquez Peraca, N., Ma, X., Jin, Z., Ren, W., Ma, G., Katayama, I., Takeda, J., Nojiri, H., Turchinovich, D., Cao, S., Bamba, M. & Kono, J. (2020), 'Magnonic quantum simulator of antiresonant ultrastrong light-matter coupling', *arXiv:2008:1234* .

Mazza, G. & Georges, A. (2019), 'Superradiant quantum materials', *Phys. Rev. Lett.* **122**, 017401.

McCombe, B. D. & Wagner, R. J. (1975), Intraband magneto-optical studies of semiconductors in the far-infrared. i, *in* L. Marton, ed., 'Advances in Electronics and Electron Physics', Vol. 37, Academic Press, New York, pp. 1–78.

Mezzacapo, A., Las Heras, U., Pedernales, J. S., DiCarlo, L., Solano, E. & Lamata, L. (2014), 'Digital quantum Rabi and Dicke models in superconducting circuits', *Sci. Rep.* **4**, 7482.

Mooradian, A. & McWhorter, A. (1967), 'Polarization and intensity of Raman scattering from

plasmons and phonons in gallium arsenide', *Phys. Rev. Lett.* **19**, 849.

Mooradian, A. & Wright, G. (1966), 'Observation of the interaction of plasmons with longitudinal optical phonons in GaAs', *Phys. Rev. Lett.* **16**, 999.

Moore, G. T. (1970), 'Quantum theory of the electromagnetic field in a variable-length one-dimensional cavity', *J. Math. Phys.* **11**, 2679–2691.

Mueller, N. S., Okamura, Y., Vieira, B. G. M., Juergensen, S., Lange, H., Barros, E. B., Schulz, F. & Reich, S. (2020), 'Deep strong light–matter coupling in plasmonic nanoparticle crystals', *Nature* **583**, 780–784.

Muravev, V. M., Andreev, I. V., Kukushkin, I. V., Schmult, S. & Dietsche, W. (2011), 'Observation of hybrid plasmon-photon modes in microwave transmission of coplanar microresonators', *Phys. Rev. B* **83**, 075309.

Muravev, V. M., Gusikhin, P. A., Andreev, I. V. & Kukushkin, I. V. (2013), 'Ultrastrong coupling of high-frequency two-dimensional cyclotron plasma mode with a cavity photon', *Phys. Rev. B* **87**, 045307.

Nataf, P., Champel, T., Blatter, G. & Basko, D. M. (2019), 'Rashba cavity QED: A route towards the superradiant quantum phase transition', *Phys. Rev. Lett.* **123**, 207402.

Nataf, P. & Ciuti, C. (2010), 'No-go theorem for superradiant quantum phase transitions in cavity QED and counter-example in circuit QED', *Nat. Commun.* **1**, 72.

Nataf, P. & Ciuti, C. (2011), 'Protected quantum computation with multiple resonators in ultrastrong coupling circuit QED', *Phys. Rev. Lett.* **107**, 190402.

Ofek, N., Petrenko, A., Heeres, R., Reinhold, P., Leghtas, Z., Vlastakis, B., Liu, Y., Frunzio, L., Girvin, S. M., Jiang, L., Mirrahimi, M., Devoret, M. H. & Schoelkopf, R. J. (2016), 'Extending the lifetime of a quantum bit with error correction in superconducting circuits', *Nature* **536**, 441–445.

Olson, C. & Lynch, D. W. (1969), 'Longitudinal-optical-phonon-plasmon coupling in GaAs', *Phys. Rev.* **177**, 1231.

Paiella, R. (2006), *Intersubband Transitions In Quantum Structures*, McGraw-Hill, New York.

Paravicini-Bagliani, G. L., Appugliese, F., Richter, E., Valmorra, F., Keller, J., Beck, M., Bartolo, N., Rössler, C., Ihn, T., Ensslin, K., Ciuti, C., Scalari, G. & Faist, J. (2018), 'Magneto-transport controlled by Landau polariton states', *Nat. Phys.* **15**, 186–190.

Paravicini-Bagliani, G. L., Scalari, G., Valmorra, F., Keller, J., Maissen, C., Beck, M. & Faist, J. (2017), 'Gate and magnetic field tunable ultrastrong coupling between a magnetoplasmon and the optical mode of an LC cavity', *Phys. Rev. B* **95**, 205304.

Parvini, T. S., Bittencourt, V. A. & Kusminskiy, S. V. (2020), 'Antiferromagnetic cavity optomagnonics', *Phys. Rev. Res.* **2**, 022027.

Pedernales, J. S., Di Candia, R., Ballester, D. & Solano, E. (2013), 'Quantum simulations of relativistic quantum physics in circuit QED', *New J. Phys.* **15**, 055008.

Perkowitz, S. & Thorland, R. (1975), 'Generalized dielectric function and the plasmon-phonon coupling in GaAs and CdTe', *Solid St. Commun.* **16**, 1093–1096.

Poddubny, A., Iorsh, I., Belov, P. & Kivshar, Y. (2013), 'Hyperbolic metamaterials', *Nat. Photon.* **7**, 948–957.

Porer, M., Ménard, J.-M., Leitenstorfer, A., Huber, R., Degl'Innocenti, R., Zanotto, S., Biasiol, G., Sorba, L. & Tredicucci, A. (2012), 'Nonadiabatic switching of a photonic band structure: Ultrastrong light-matter coupling and slow-down of light', *Phys. Rev. B* **85**, 081302(R).

Puebla, R., Hwang, M.-J., Casanova, J. & Plenio, M. B. (2017), 'Probing the dynamics of a superradiant quantum phase transition with a single trapped ion', *Phys. Rev. Lett.* **118**, 073001.

Quattropani, A. & Schwendimann, P. (2005), 'Polariton squeezing in microcavities', *phys. stat. sol. (b)* **242**, 2302–2314.

Raines, Z. M., Allocca, A. A., Hafezi, M. & Galitski, V. M. (2020), 'Cavity Higgs polaritons', *Phys.*

Rev. Res. **2**, 013143.

Rajabali, S., Scalari, G., Keller, J., Beck, M. & Faist, J. (2019), The upper branch broadening in ultrastrongly coupled thz landau polaritons, *in* 'Proc. of the 44th Int. Conf. Infrared, Millimeter, and Terahertz Waves (IRMMW-THz)', IEEE, pp. 1–1.

Ridolfo, A., Leib, M., Savasta, S. & Hartmann, M. J. (2012), 'Photon blockade in the ultrastrong coupling regime', *Phys. Rev. Lett.* **109**, 193602.

Romero, G., Ballester, D., Wang, Y. M., Scarani, V. & Solano, E. (2012), 'Ultrafast quantum gates in circuit QED', *Phys. Rev. Lett.* **108**, 120501.

Roth, M., Hassler, F. & DiVincenzo, D. P. (2019), 'Optimal gauge for the multimode Rabi model in circuit QED', *Phys. Rev. Res.* **1**, 033128.

Rzażewski, K., Wódkiewicz, K. & Żakowicz, W. (1975), 'Phase transitions, two-level atoms, and the A^2 term', *Phys. Rev. Lett.* **35**, 432–434.

Sachet, E., Shelton, C. T., Harris, J. S., Gaddy, B. E., Irving, D. L., Curtarolo, S., Donovan, B. F., Hopkins, P. E., Sharma, P. A., Sharma, A. L. et al. (2015), 'Dysprosium-doped cadmium oxide as a gateway material for mid-infrared plasmonics', *Nat. Mater.* **14**, 414–420.

Sanchez-Burillo, E., Zueco, D., Garcia-Ripoll, J. J. & Martin-Moreno, L. (2014), 'Scattering in the ultrastrong regime: Nonlinear optics with one photon', *Phys. Rev. Lett.* **113**, 263604.

Sapienza, L., Vasanelli, A., Ciuti, C., Manquest, C., Sirtori, C., Colombelli, R. & Gennser, U. (2007), 'Photovoltaic probe of cavity polaritons in a quantum cascade structure', *Appl. Phys. Lett.* **90**, 201101.

Sapienza, L., Vasanelli, A., Colombelli, R., Ciuti, C., Chassagneux, Y., Manquest, C., Gennser, U. & Sirtori, C. (2008), 'Electrically injected cavity polaritons', *Phys. Rev. Lett.* **100**, 136806.

Scalari, G., Maissen, C., Hagenmüller, D., De Liberato, S., Ciuti, C., Reichl, C., Wegscheider, W., Schuh, D., Beck, M. & Faist, J. (2013), 'Ultrastrong light-matter coupling at terahertz frequencies with split ring resonators and inter-Landau level transitions', *J. Appl. Phys.* **113**, 136510.

Scalari, G., Maissen, C., Turčinková, D., Hagenmüller, D., De Liberato, S., Ciuti, C., Reichl, C., Schuh, D., Wegscheider, W., Beck, M. & Faist, J. (2012), 'Ultrastrong coupling of the cyclotron transition of a 2D electron gas to a THz metamaterial', *Science* **335**, 1323–1326.

Schlawin, F., Cavalleri, A. & Jaksch, D. (2019), 'Cavity-mediated electron-photon superconductivity', *Phys. Rev. Lett.* **122**, 133602.

Schneider, H. & Liu, H. C. (2007), *Quantum well infrared photodetectors*, Springer, Berlin.

Schuler, M., De Bernardis, D., Läuchli, A. M. & Rabl, P. (2020), 'Cavity quantum electrodynamics of strongly correlated dipolar matter', *arXiv:2004.13738* .

Schwendimann, P. & Quattropani, A. (1992*a*), 'Nonclassical properties of polariton states', *Europhys. Lett.* **17**, 355–358.

Schwendimann, P. & Quattropani, A. (1992*b*), 'Nonclassical properties of polariton states', *Europhys. Lett.* **18**, 281–281.

Sentef, M. A., Ruggenthaler, M. & Rubio, A. (2018), 'Cavity quantum-electrodynamical polaritonically enhanced electron-phonon coupling and its influence on superconductivity', *Sci. Adv.* **4**, eaau6969.

Shang, Q., Zhang, S., Liu, Z., Chen, J., Yang, P., Li, C., Li, W., Zhang, Y., Xiong, Q., Liu, X. et al. (2018), 'Surface plasmon enhanced strong exciton–photon coupling in hybrid inorganic–organic perovskite nanowires', *Nano Lett.* **18**, 3335–3343.

Shapiro, D. S., Zhukov, A. A., Pogosov, W. V. & Lozovik, Y. E. (2015), 'Dynamical Lamb effect in a tunable superconducting qubit-cavity system', *Phys. Rev. A* **91**, 1–10.

Shirley, J. H. (1965), 'Solution of the Schrödinger equation with a Hamiltonian periodic in time', *Phys. Rev.* **138**, B979–B987.

Singwi, K. & Tosi, M. (1966), 'Interaction of plasmons and optical phonons in degenerate semicon-

ductors', *Phys. Rev.* **147**, 658.

Skolnick, M. S., Fisher, T. A. & Whittaker, D. M. (1998), 'Strong coupling phenomena in quantum microcavity structures', *Semicond. Sci. Technol.* **13**, 645–669.

Stassi, R., Ridolfo, A., Di Stefano, O., Hartmann, M. J. & Savasta, S. (2013), 'Spontaneous conversion from virtual to real photons in the ultrastrong-coupling regime', *Phys. Rev. Lett.* **110**, 243601.

Stassi, R., Savasta, S., Garziano, L., Spagnolo, B. & Nori, F. (2016), 'Output field-quadrature measurements and squeezing in ultrastrong cavity-QED', *New J. Phys.* **18**, 123005.

Stefano, O. D., Stassi, R., Garziano, L., Kockum, A. F., Savasta, S. & Nori, F. (2017), 'Feynman-diagrams approach to the quantum Rabi model for ultrastrong cavity QED: Stimulated emission and reabsorption of virtual particles dressing a physical excitation', *New J. Phys.* **19**, 053010.

Stokes, A. & Nazir, A. (2019*a*), 'Gauge ambiguities imply Jaynes-Cummings physics remains valid in ultrastrong coupling QED', *Nat. Commun.* **10**, 499.

Stokes, A. & Nazir, A. (2019*b*), 'Ultrastrong time-dependent light-matter interactions are gauge-relative', *arXiv:1902.05160* .

Stokes, A. & Nazir, A. (2019*c*), 'Uniqueness of the phase transition in many-dipole cavity QED systems', *arXiv:1905.10697* .

Su, R., Diederichs, C., Wang, J., Liew, T. C., Zhao, J., Liu, S., Xu, W., Chen, Z. & Xiong, Q. (2017), 'Room-temperature polariton lasing in all-inorganic perovskite nanoplatelets', *Nano Lett.* **17**, 3982–3988.

Su, R., Ghosh, S., Wang, J., Liu, S., Diederichs, C., Liew, T. C. & Xiong, Q. (2020), 'Observation of exciton polariton condensation in a perovskite lattice at room temperature', *Nat. Phys.* **16**, 301–306.

Su, R., Wang, J., Zhao, J., Xing, J., Zhao, W., Diederichs, C., Liew, T. C. & Xiong, Q. (2018), 'Room temperature long-range coherent exciton polariton condensate flow in lead halide perovskites', *Sci. Adv.* **4**, eaau0244.

Sun, Z., Fogler, M. M., Basov, D. N. & Millis, A. J. (2020), 'Collective modes and terahertz near-field response of superconductors', *Phys. Rev. Res.* **2**, 023413.

Sun, Z., Gu, J., Ghazaryan, A., Shotan, Z., Considine, C. R., Dollar, M., Chakraborty, B., Liu, X., Ghaemi, P., Kéna-Cohen, S. et al. (2017), 'Optical control of room-temperature valley polaritons', *Nat. Photon.* **11**, 491.

Tabuchi, Y., Ishino, S., Ishikawa, T., Yamazaki, R., Usami, K. & Nakamura, Y. (2014), 'Hybridizing ferromagnetic magnons and microwave photons in the quantum limit', *Phys. Rev. Lett.* **113**, 083603.

Thomas, A., Devaux, E., Nagarajan, K., Chervy, T., Seidel, M., Hagenmüller, D., Schütz, S., Schachenmayer, J., Genet, C., Pupillo, G. et al. (2019), 'Exploring superconductivity under strong coupling with the vacuum electromagnetic field', *arXiv:1911.01459* .

Tobar, M. E. & Goryachev, M. (2019), 'Microwave frequency magnetic field manipulation systems and methods and associated application instruments, apparatus and system'. US Patent 10,290,916.

Todorov, Y. (2014), 'Dipolar quantum electrodynamics theory of the three-dimensional electron gas', *Phys. Rev. B* **89**, 75115.

Todorov, Y., Andrews, A. M., Colombelli, R., De Liberato, S., Ciuti, C., Klang, P., Strasser, G. & Sirtori, C. (2010), 'Ultrastrong light-matter coupling regime with polariton dots', *Phys. Rev. Lett.* **105**, 196402.

Todorov, Y., Andrews, A., Sagnes, I., Colombelli, R., Klang, P., Strasser, G. & Sirtori, C. (2009), 'Strong light-matter coupling in subwavelength metal-dielectric microcavities at terahertz frequencies', *Phys. Rev. Lett.* **102**, 186402.

Todorov, Y. & Sirtori, C. (2012), 'Intersubband polaritons in the electrical dipole gauge', *Phys. Rev. B* **85**, 45304.

Todorov, Y. & Sirtori, C. (2014), 'Few-electron ultrastrong light-matter coupling in a quantum LC circuit', *Phys. Rev. X* **4**, 041031.

Todorov, Y., Tosetto, L., Teissier, J., Andrews, A. M., Klang, P., Colombelli, R., Sagnes, I., Strasser, G. & Sirtori, C. (2010), 'Optical properties of metal-dielectric-metal microcavities in the THz fquency range', *Opt. Express* **18**, 13886–13907.

Tokura, Y., Kawasaki, M. & Nagaosa, N. (2017), 'Emergent functions of quantum materials', *Nat. Phys.* **13**, 1056–1068.

Unruh, W. G. (1974), 'Second quantization in the Kerr metric', *Phys. Rev. D* **10**, 3194–3205.

Unruh, W. G. (1976), 'Notes on black-hole evaporation', *Phys. Rev. D* **14**, 870–892.

van Vugt, L. K., Rühle, S., Ravindran, P., Gerritsen, H. C., Kuipers, L. & Vanmaekelbergh, D. (2006), 'Exciton polaritons confined in a ZnO nanowire cavity', *Phys. Rev. Lett.* **97**, 147401.

Varga, B. B. (1965), 'Coupling of plasmons to polar phonons in degenerate semiconductors', *Phys. Rev.* **137**, A1896.

Viehmann, O., von Delft, J. & Marquardt, F. (2011), 'Superradiant phase transitions and the standard description of circuit QED', *Phys. Rev. Lett.* **107**, 113602.

Vukics, A. & Domokos, P. (2012), 'Adequacy of the Dicke model in cavity QED: A counter-no-go statement', *Phys. Rev. A* **86**, 53807.

Vukics, A., Grießer, T. & Domokos, P. (2014), 'Elimination of the *A*-square problem from cavity QED', *Phys. Rev. Lett.* **112**, 073601.

Vukics, A., Grießer, T. & Domokos, P. (2015), 'Fundamental limitation of ultrastrong coupling between light and atoms', *Phys. Rev. A* **92**, 043835.

Wang, J., Su, R., Xing, J., Bao, D., Diederichs, C., Liu, S., Liew, T. C., Chen, Z. & Xiong, Q. (2018), 'Room temperature coherently coupled exciton–polaritons in two-dimensional organic–inorganic perovskite', *ACS Nano* **12**, 8382–8389.

Wang, T., Li, P., Hauer, B., Chigrin, D. N. & Taubner, T. (2013), 'Optical properties of single infrared resonant circular microcavities for surface phonon polaritons', *Nano Lett.* **13**, 5051–5055.

Wang, X., Ronca, E. & Sentef, M. A. (2019), 'Cavity quantum electrodynamical Chern insulator: Towards light-induced quantized anomalous Hall effect in graphene', *Phys. Rev. B* **99**, 235156.

Wang, Y.-D., Chesi, S., Loss, D. & Bruder, C. (2010), 'One-step multiqubit Greenberger-Horne-Zeilinger state generation in a circuit QED system', *Phys. Rev. B* **81**, 104524.

Wang, Y. K. & Hioe, F. T. (1973), 'Phase transition in the Dicke model of superradiance', *Phys. Rev. A* **7**, 831–836.

Wang, Y., Zhang, J., Wu, C., You, J. Q. & Romero, G. (2016), 'Holonomic quantum computation in the ultrastrong-coupling regime of circuit QED', *Phys. Rev. A* **94**, 012328.

Wei, H.-S., Jaing, C.-C., Chen, Y.-T., Lin, C.-C., Cheng, C.-W., Chan, C.-H., Lee, C.-C. & Chang, J.-F. (2013), 'Adjustable exciton-photon coupling with giant Rabi-splitting using layer-by-layer J-aggregate thin films in all-metal mirror microcavities', *Opt. Exp.* **21**, 21365–21373.

Weisbuch, C., Nishioka, M., Ishikawa, A. & Arakawa, Y. (1992), 'Observation of the coupled exciton-photon mode splitting in a semiconductor quantum microcavity', *Phys. Rev. Lett.* **69**, 3314–3317.

West, L. & Eglash, S. (1985), 'First observation of an extremely large-dipole infrared transition within the conduction band of a GaAs quantum well', *Appl. Phys. Lett.* **46**, 1156–1158.

Wilson, C. M., Johansson, G., Pourkabirian, A., Simoen, M., Johansson, J. R., Duty, T., Nori, F. & Delsing, P. (2011), 'Observation of the dynamical Casimir effect in a superconducting circuit', *Nature* **479**(7373), 376–379.

Woolley, R. G. (1976), 'Gauge invariance and the thermodynamics of the electromagnetic field', *J. Phys. A. Math. Gen.* **9**, L15–L16.

Yablonovitch, E. (1989), 'Accelerating reference frame for electromagnetic waves in a rapidly growing plasma: Unruh-Davies-Fulling-DeWitt radiation and the nonadiabatic Casimir effect', *Phys. Rev. Lett.* **62**, 1742–1745.

Yamanoi, M. (1976), 'Influence of omitting the A^2 term in the conventional photon-matter-Hamiltonian on the photon-field equation', *Phys. Lett. A* **58**, 437 – 439.

Yamanoi, M. & Takatsuji, M. (1978), Influence of omitting the P^2 term in the multipole photon-matter Hamiltonian on the stability and propagation, *in* L. Mandel & E. Wolf, eds, 'Coherence Quantum Opt. IV Proc. Fourth Rochester Conf. Coherence Quantum Opt.', Plenum Press, New York, pp. 839–850.

Yee, C. M. & Sherwin, M. S. (2009), 'High-Q terahertz microcavities in silicon photonic crystal slabs', *Appl. Phys. Lett.* **94**.

Yokota, I. (1961), 'On the coupling between optical lattice vibrations and carrier plasma oscillations in polar semiconductors', *J. Phys. Soc. Jpn* **16**, 2075–2075.

Yoo, D., de León-Pérez, F., Lee, I.-H., Mohr, D. A., Pelton, M., Raschke, M. B., Caldwell, J. D., Martín-Moreno, L. & Oh, S.-H. (2020), 'Ultrastrong coupling of polar phonons and effective epsilon-near-zero modes in coaxial nanocavities', *arXiv:2003.00136* .

Yoshihara, F., Fuse, T., Ashhab, S., Kakuyanagi, K., Saito, S. & Semba, K. (2017), 'Superconducting qubit-oscillator circuit beyond the ultrastrong-coupling regime', *Nat. Phys.* **13**, 44–47.

Yoshioka, D. (2002), *The Quantum Hall Effect*, Springer, Berlin and New York.

Yoxall, E., Schnell, M., Nikitin, A. Y., Txoperena, O., Woessner, A., Lundeberg, M. B., Casanova, F., Hueso, L. E., Koppens, F. H. & Hillenbrand, R. (2015), 'Direct observation of ultraslow hyperbolic polariton propagation with negative phase velocity', *Nat. Photon.* **9**, 674–678.

Zanotto, S., Biasiol, G., Degl'Innocenti, R., Sorba, L. & Tredicucci, A. (2010), 'Intersubband polaritons in a one-dimensional surface plasmon photonic crystal', *Appl. Phys. Lett.* **97**, 231123.

Zanotto, S., Degl'Innocenti, R., Xu, J.-H., Sorba, L., Tredicucci, A. & Biasiol, G. (2012), 'Ultrafast optical bleaching of intersubband cavity polaritons', *Phys. Rev. B* **86**, 201302.

Zhang, Q., Arikawa, T., Kato, E., Reno, J. L., Pan, W., Watson, J. D., Manfra, M. J., Zudov, M. A., Tokman, M., Erukhimova, M., Belyanin, A. & Kono, J. (2014), 'Superradiant decay of cyclotron resonance of two-dimensional electron gases', *Phys. Rev. Lett.* **113**, 047601.

Zhang, Q., Lou, M., Li, X., Reno, J. L., Pan, W., Watson, J. D., Manfra, M. J. & Kono, J. (2016), 'Collective non-perturbative coupling of 2D electrons with high-quality-factor terahertz cavity photons', *Nat. Phys.* **12**, 1005–1011.

Zhang, S., Shang, Q., Du, W., Shi, J., Wu, Z., Mi, Y., Chen, J., Liu, F., Li, Y., Liu, M. et al. (2018), 'Strong exciton–photon coupling in hybrid inorganic–organic perovskite micro/nanowires', *Adv. Opt. Mater.* **6**, 1701032.

Zhang, X., Galda, A., Han, X., Jin, D. & Vinokur, V. (2020), 'Broadband nonreciprocity enabled by strong coupling of magnons and microwave photons', *Phys. Rev. Applied* **13**, 044039.

Zhang, X., Zhu, N., Zou, C.-L. & Tang, H. X. (2016), 'Optomagnonic whispering gallery microresonators', *Phys. Rev. Lett.* **117**, 123605.

Zhang, X., Zou, C.-L., Jiang, L. & Tang, H. X. (2014), 'Strongly coupled magnons and cavity microwave photons', *Phys. Rev. Lett.* **113**, 156401.

Zhong, Y., Malagari, S. D., Hamilton, T. & Wasserman, D. M. (2015), 'Review of mid-infrared plasmonic materials', *J. Nanophoton.* **9**, 093791.